Methodological approach to the assessment of commercial materials for additive manufacturing

Kovačić, Ivan Goran

SVEUČILIŠTE U RIJECI

TEHNIČKI FAKULTET

Diplomski sveučilišni studij strojarstva

Diplomski rad

METODOLOŠKI PRISTUP PROCJENI KOMERCIJALNIH MATERIJALA ZA ADITIVNU PROIZVODNJU

Rijeka, 10. rujan 2024.

Ivan Goran Kovačić

0069060007

SVEUČILIŠTE U RIJECI

TEHNIČKI FAKULTET

Diplomski sveučilišni studij strojarstva

Diplomski rad

METODOLOŠKI PRISTUP PROCJENI KOMERCIJALNIH MATERIJALA ZA ADITIVNU PROIZVODNJU

Mentorica: izv. prof. dr. sc. Kristina Marković

Komentorica: Maja Dundović, dipl. ing.

Rijeka, 10. rujan 2024.

Ivan Goran Kovačić

0069060007

SVEUČILIŠTE U RIJECI
TEHNIČKI FAKULTET
POVJERENSTVO ZA DIPLOMSKE ISPITE

Rijeka, 19.06.2024.

Zavod: Zavod za konstruiranje

Predmet: Konstrukcijski elementi robota

ZADATAK ZA DIPLOMSKI RAD

Pristupnik: **Ivan Goran Kovačić (0069060007)**

Studij: Sveučilišni diplomski studij strojarstva (2100)

Modul: Konstruiranje i mehatronika (2111)

Zadatak: **Metodološki pristup procjeni komercijalnih materijala za aditivnu proizvodnju / Methodological approach to the assessment of commercial materials for additive manufacturing**

Opis zadatka:

Obzirom na sve prisutniju uporabu komercijalnih materijala za aditivnu proizvodnju, rad treba pokriti istraživanje njihovog ponašanja u cilju davanja smjernica za njihovu primjenu. S tim u vezi potrebno je ispitati ponašanje aditivno proizvedenih ispitnih uzoraka iz PLA i PETG materijala eksperimentalnim vlačnim testovima. Odziv materijala potrebno je bilježiti za uzroke izrađene na različitim uređajima i to za različito postavljene proizvodne postavke. Potrebno je provesti analizu utjecaja uređaja za aditivnu proizvodnju na mehanička svojstva materijala te analizu utjecaja broja uzoraka na njihovu nosivost obzirom na međuslojne veze. Rad treba sadržavati i razvoj numeričkog modela za simulaciju ponašanja promatranih materijala te zaključno smjernice za primjenu rezultata istraživanja na robotske komponente.

Rad mora biti napisan prema Uputama za pisanja diplomskih / završnih radova koje su objavljene na mrežnim stranicama studija.

Zadatak uručen pristupniku: 20.03.2024.

Predsjednik povjerenstva za diplomski ispit:
izv. prof. dr. sc. Igor Bonefačić

Mentor:
izv. prof. dr. sc. Kristina Marković

Komentor:
Maja Dundović

IZJAVA

Sukladno članku 9. pravilnika o završnom radu, završnom ispitu i završetku preddiplomskih sveučilišnih studija Tehničkog fakulteta Sveučilišta u Rijeci iz lipnja 2011. godine, izjavljujem da sam samostalno izradio diplomski rad „Metodološki pristup procjeni komercijalnih materijala za aditivnu proizvodnju“ pod vodstvom mentorice izv. prof. dr. sc. Kristina Marković i komentorice Maja Dundović, dipl. ing. Rad je rađen od 05. srpnja 2024. do 3. rujna 2024. godine. Koristio sam vlastito iskustveno znanje, pomoć mentorica i literaturu navedenu na kraju rada.
Methodological approach to the assessment of commercial materials for additive manufacturing

_____

Ivan Goran Kovačić
0069060007

U Rijeci, rujan 2024.

Zahvala

Ovim putem zahvaljujem mentorici izv. prof. dr. sc. Kristina Marković i komentorici Maja Dundović, dipl. ing. na suradnji, susretljivosti te savjetima koje su mi davali tijekom izrade ovog diplomskog rada. Njihovim vođenjem i smjernicama su mi pomogle pri razumijevanju i izradi, kako teoretskog, tako i praktičnog dijela zadatka. Također, zahvaljujem i ostalim djelatnicima Zavoda za konstruiranje pri pomoći na izradi eksperimentalnog dijela rada.

CONTENTS

1. INTRODUCTION

The rapid adoption of 3D printing technologies, particularly Fused Deposition Modeling (FDM), for manufacturing consumer products and robotics parts has raised important questions about the mechanical reliability of 3D-printed parts. Unlike traditional manufacturing methods, FDM involves layer-by-layer deposition, which results in anisotropic properties. This anisotropy, along with factors such as layer adhesion and surface roughness, complicates the prediction and consistency of material performance. As the technology continues to evolve, there is a growing need to optimize print parameters and make suitable numerical models that can accurately predict its material properties [1].

This paper aims to investigate the differences in material properties of parts produced using various FDM setups and part build orientations, focusing specifically on the interfacial bonding strength (IFBS) of commercially available materials like PLA and PETG. To gather representative and comparative results, testing procedure ISO 527 was followed. By conducting tensile tests on specimens made in different conditions, including variations in build orientation and time to print one layer; the study provides deeper insights into how these parameters influence the overall material properties of FDM parts. Understanding these influences is crucial for developing more accurate material models which can reliably predict the mechanical behaviour of FDM-printed components.

The objective of this research is to collect representative data, such as Young's modulus and ultimate strength, in order to develop a numerical model that can reliably predict the material properties of 3D-printed parts. To test the hypothesis that 3D-printed components can be accurately represented through numerical models derived from simplified geometries, Finite Element Analysis (FEA) was conducted. The model was designed to include two isotropic materials: one representing the extruded filament lines, and the other functioning as a bonding element between the layers. This bonding element simulates IFBS, often referred to as the 'glue' that holds the layers together. This dual-material approach enhances the accuracy of the numerical model in capturing the complex mechanical behaviour of FDM-printed parts.

In the final part of the paper, a few guidelines are provided for successful 3D printing, focusing on how the insights from this study can be used to predict material properties and print significantly stronger robotic parts.

2. LITERATURE OVERVIEW

FDM is an extrusion-based 3D printing technique that uses polymer filaments as the material, which are heated, melted, and deposited layer by layer to form a 3D object. In some papers also referred as fused filament fabrication (FFF) [2] or material extrusion additive manufacturing (MEAM) [3]. It is the most commonly used additive manufacturing (AM) technique due to its availability, low-cost and ease of operation. FDM is important for robotics because it enables the rapid prototyping of custom parts at a low cost, allowing for design iterations and optimizations. Additionally, it supports the production of lightweight, durable components tailored to specific robotic functions

Research on FDM focuses extensively on optimizing design, understanding the effects of process parameters, and enhancing the material properties of printed parts. The anisotropy results from the layer-by-layer printing process leads to different mechanical properties in various directions. In this part, state of the industry and it's main areas are presented [4].

Key Research Areas

- Material Development: new composite materials and high-performance polymers to improve part strength, thermal stability, and durability. The use of fiber-reinforced materials like ABS/CF-PLA composites shows promising results in enhancing mechanical properties of FDM-s [5].
- Process Optimization: process parameters such as layer thickness, raster angle, infill density, print speed, extrusion temperature, and air gap significantly affect the mechanical properties and quality of FDM prototypes [6] [7].
- Multi-Material Printing: Printing with multiple materials to create parts with enhanced functionality and mechanical properties, such as varying stiffness or conductivity within a single part [4].

Critical Parameters Affecting FDM Parts:

- Layer Thickness and Orientation: Influence surface finish, strength, and accuracy.
- Print Speed and Extrusion Temperature: Affect bonding quality and overall part strength [7].

- Infill Density and Pattern: Dictate the internal structure's strength and weight.
- Nozzle Diameter: Impacts resolution and detail of printed parts [8].

Research often focuses on improving mechanical properties such as tensile strength, impact resistance, and flexural strength, as well as thermal properties for applications requiring heat resistance. The anisotropic nature of FDM parts necessitates specific design and process considerations to ensure consistent performance across different directions [6].

FDM is a complex process with many conflicting parameters that influence part quality and material properties (Figure 2.1. shows main parameters that affect FDM properties). Due to the absence of specific standards for mechanical testing of FDM parts, there is considerable variability in research methodologies, leading to disagreements on the influence of different parameters [3].

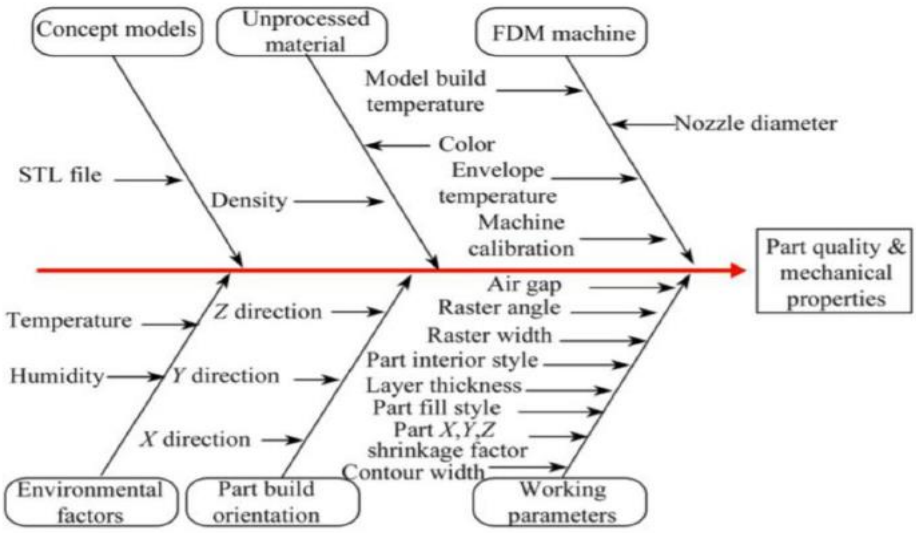

Figure 2.1. Main parameters that affect AM FDM properties [9]

Research in FDM additive manufacturing is highly multidisciplinary, involving material science, mechanical engineering, and computer science. The ongoing work aims to optimize print parameters, enhance material properties, and develop new applications to expand the capabilities and applicability of FDM in industrial, medical, and consumer markets.

3. TESTING METHODOLOGY

This section of the paper presents the testing methodology. The entire experiment follows the procedure defined by ISO 527 [9]. First, the equipment used in the experiment is introduced, including 3D printers, a universal testing machine with its necessary components, and a microscopic camera. The test specimens are then detailed, followed by the printing plan. The testing procedure is explained, covering key concepts such as stress, strain, their properties, and characteristic plots. Printing parameters and post-processing of the printed specimens are described. A detailed tensile testing procedure is provided, followed by an examination of the metallographic cuts of the fractured specimens. Metallographic analysis was performed to investigate the internal structure of the printed parts, and the data obtained from these experiments will be used to develop a numerical model that accurately predicts the behaviour of FDM-printed components.

3.1 Equipment, testing material and specimens

This section describes the primary equipment used in the experiments, including the 3D printers and the universal testing machine. It also details the materials selected for printing and the specifications of the test specimens used in the study. These elements are crucial for ensuring consistent and accurate testing of material properties under the experimental conditions.

Two materials were chosen to test on; Polylactic Acid (PLA) and Polyethylene Terephthalate Glycol (PETG). PLA is among the most widely used materials in 3D printing, particularly favored in extrusion-based 3D printers. Its popularity stems from its ease of use, as PLA can be printed at relatively low temperatures and does not necessitate a heated bed [10]. PETG is also popular choice for filaments and FDM as it combines both the simplicity of PLA printing and the strength of ABS [11]. Same series of filament rolls were used for printing all specimens. Prusament PLA series PRM-PLA-GLX-1000 date of production 09.09.2023. and Prusament PET G series PRM-PETG-GLX-1000 date of production 21.09.2023.

3.1.1 Printers

Testing samples type 1A defined by ISO 527 were designed in 3D CAD modelling software *SolidWorks*. It was then exported to STEP format that was loaded into software *PrusaSlicer.* That is slicing software specifically designed to convert 3D models into instructions (G-code) that FDM 3D printers can understand and execute. In this experiment Prusa MKS3 [12] and TRILAB AzteQ Industrial [13] are used.

The Prusa MK3S (Figure 3.1.) features a Cartesian motion system and an open build chamber, making it suitable for general-purpose applications, including prototyping and small-scale manufacturing [14]. It supports a wide range of materials (e.g., PLA, PETG, ABS) and incorporates features like a direct drive extruder, automated mesh bed levelling, and power loss recovery, which enhance its reliability and print quality. Its user-friendly interface and broad community support make it ideal for hobbyists, educators, and small businesses [12].

Figure 3.1. Prusa i3 mk3s 3D printer [12]

The TRILAB AzteQ Industrial (Figure 3.2.) utilizes a Delta kinematic system, providing higher speed, precision and smoother motion, particularly for complex geometries [15]. It features an enclosed build chamber, allowing for controlled thermal environments necessary for printing high-temperature

engineering plastics such as ABS and ASA. Its modular design, advanced monitoring capabilities, and broad material compatibility make it well-suited for industrial applications where precision, material versatility, and operational reliability are critical [13].

Figure 3.2. TRILAB AzteQ Industrial [13]

While the Prusa MK3S+ is optimized for ease of use and versatility across various standard materials, the TRILAB AzteQ Industrial is designed for professional settings demanding high performance and material flexibility. They were chosen to do the tests on exactly because they are designed for different user bases and operational contexts.

3.1.2 Test specimens

Test specimens are dumb-bell-shaped types 1A from ISO 527, as shown in Figure 3.3. The middle region of the specimen is intentionally designed to be narrower, ensuring that if necking occurs, the wider sections of the specimen will compensate for it, allowing the measurement process to continue using head displacement.

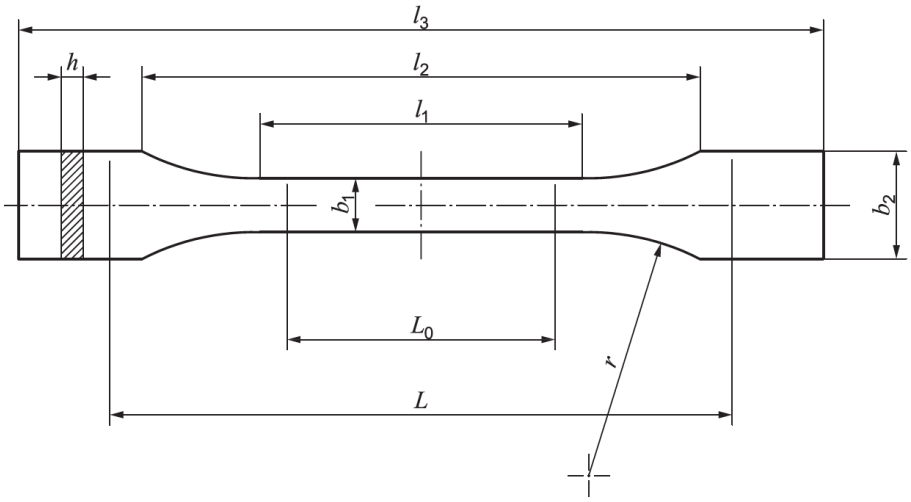

Figure 3.3. Shape of test specimen type 1A [16]

The specimen dimensions and their corresponding allowable tolerances are presented in Table 3.1.

Table 3.1. Dimensions of test specimen type 1A [16]

l_3	Overall length	170 mm
l_1	length of narrow parallel-sided portion	80 ±2 mm
r	Radius	24 ±1 mm
l_2	Distance between broad parallel-sided portions	109,3 ±3,2 mm
b_2	Width at ends	20 ±0,2 mm
b_1	Width at narrow portion	10 ±0,2 mm
h	Thickness	4 ±0,2 mm
L_0	Gauge length	50 ±0,5 mm
L	Initial distance between grips	115 ±1 mm

Figure 3.4. Shows example of printed samples. On the left of Fig. 3.4. is single vertical specimen on Prusa and PLA material from series 1, and right are series 6; printed on AzteQ, five specimens at once horizontally, PLA material.

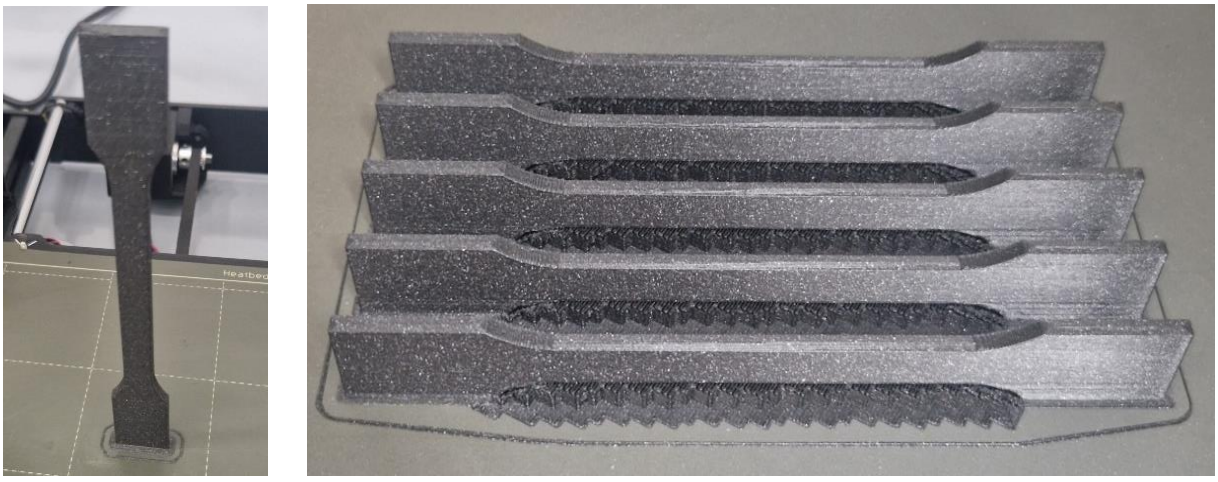

Figure 3.4. Left - single vertical specimen on Prusa, right - five horizontal specimen on AzteQ

3.1.3 Universal testing machine

Tensile strength is determined by universal testing machine (UTM), also known as a universal tester [17]. UTM used for this experiment is a STEP Lab EA100 [18]. It is dynamic testing machine based on electromechanical actuators. The machine complies with both ISO 7500-1 and ISO 9513 and meets the specifications of test speeds and required tolerances. The force measurement system complies with class 1 as defined in ISO 7500-1:2004 [18].

On Figure 3.5. is shown machine used and its surrounding parts needed for function; machine by itself, computer for data acquisition, pneumatic system provides air for clamping grippers, pedals for controlling each grip individually and left on picture is UTM supporting controller.

Figure 3.5. STEP Lab universal testing machine

Grips designed to hold the test specimen are secured to the testing machine, ensuring that the major axis of the specimen aligns with the direction of extension along the centerline of the grip assembly. The specimen is clamped in such a way that prevents any slippage relative to the gripping jaws, ensuring accurate measurement of tensile properties. Attention was taken to ensure adequate gripping force. Grips clamp with a help of air pressure [9]. Pressure was adjusted so it held specimen in place but didn't cause premature fracture at the jaws or squashing of the specimen in the grips. That was achieved with atmospheric pressure of 5 bars.

An extensometer is a device used for measuring strain, specifically the extension of a specimen under load [19]. In this study, an Epsilon 3442 extensometer is used, as shown in Figure 3.6. This miniature contact extensometer complies with ISO 9513:1999, class 1 standards [20], ensuring high accuracy over the strain range in which measurements are taken. To accurately determine the tensile modulus (E_t), it is essential to use an instrument capable of measuring changes in gauge length with an accuracy of 1% of the relevant value or better, as specified by the standard. While a gauge length of 75 mm is preferred due to its higher accuracy, a gauge length of 50 mm is also considered acceptable [9].

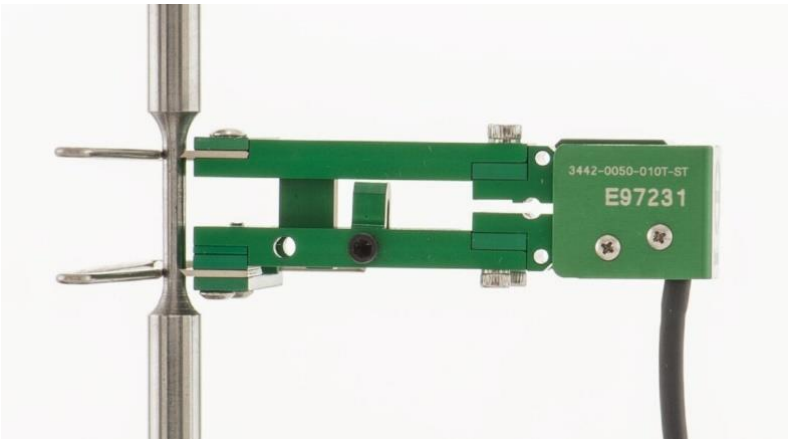

Figure 3.6. Extensometer Epsilon 3442 [20]

Recording of Data

During testing, force and the corresponding changes in gauge length, as well as the distance between grips, were automatically recorded. The data acquisition frequency must be sufficiently high to ensure compliance with accuracy requirements.

The required data acquisition frequency for recording depends on several factors:

- v - test speed, expressed in mm/min.
- $\frac{L_0}{L}$ - the ratio of the gauge length to the initial grip-to-grip separation.
- r - minimum resolution of the strain signal necessary to achieve accurate measurements, typically set to half the required accuracy value or better [mm] [9].

The minimum data acquisition frequency, f_{min} (in Hz), required for accurate transmission from the sensor to the indicator, is calculated as:

$$f_{min} = \frac{v}{60} \cdot \frac{L_0}{L \cdot r} \tag{3.1}$$

Extensometer used has biggest gauge length of 50 mm and resolution of 0.0001 mm. That is what is used in calculation of needed acquisition frequency:

$$f_{min} = \frac{v}{60} \cdot \frac{L_0}{L * r} = \frac{1\ mm/min}{60\ s/min} \cdot \frac{50\ mm}{115\ mm \cdot 0.0001\ mm} = 72{,}46\ Hz$$

The recording frequency of the test machine shall be at least equal to this data rate f_{min}. Considering this, it's chosen 100 Hz data sample rate for testing on UTM.

For the measurement of the tensile modulus, ISO 527 specifies that the testing speed should be 1 mm/min for specimen type 1A. Once the stresses required for determining the tensile modulus (up to a strain of $\varepsilon_2 = 0.25$ %) are obtained, the same test specimen can be used to continue testing at a higher speed [9]. To streamline the testing procedure, a constant test speed of 1 mm/min was maintained throughout the entire testing process for all specimens.

3.2 Printing plan

For planning series that will be printed, initially Design of Experiment (DOE) was considered, but for specific parameters being tested in this paper it deemed more appropriate making a design of experiment ourselves.

To obtain representative results, all testing was conducted in accordance with ISO 527, with additional constraints to ensure consistency. All test samples were printed using the same series of filament spools, under identical testing conditions and printing parameters. These limitations were applied to ensure reproducibility while balancing the practical considerations of print time and feasibility.

A detailed printing plan was developed to account for these factors and is presented in Table 3.2. A total of 142 specimens were printed and subjected to tensile testing. The theoretical continuous print time required to produce all 22 series was 314 hours. However, the actual print time was higher, as some series had to be reprinted due to insufficient part print quality.

Table 3.2. Printing plan

					# of printed specimens			Filament usage [g]		Time [h]	
Series	**Material**	**Printer**	**Orientation**	t_1 **[sec]**	Per print	Repeat	Sum	Per sample	Sum	Per sample	Sum
1	PLA	Prusa	Horizontal	60	1	5	5	13,4	66,9	1:58	9:50
2	PLA	Prusa	Horizontal	180	3	1	3	13,4	13,4	5:54	5:54
3	PLA	Prusa	Horizontal	300	5	1	5	13,4	13,4	9:50	9:50
4	PLA	TRILAB	Horizontal	60	1	5	5	13,4	66,9	1:58	9:50
5	PLA	TRILAB	Horizontal	180	3	1	3	13,4	13,4	5:54	5:54
6	PLA	TRILAB	Horizontal	300	5	1	5	13,4	13,4	9:50	9:50
7	PLA	Prusa	Vertical	5	1	5	5	11,9	59,3	1:50	9:10
8	PLA	Prusa	Vertical	20	11	1	11	11,9	11,9	20:54	20:54
9	PLA	TRILAB	Vertical	40	1	5	5	11,9	59,3	1:50	9:10
10	PLA	TRILAB	Vertical	60	11	1	11	11,9	11,9	20:54	20:54
11	PLA	Prusa	Vertical	5	4	2	8	11,9	23,7	7:29	14:58
12	PLA	TRILAB	Vertical	20	4	2	8	11,9	23,7	7:29	14:58
13	PLA	Prusa	Vertical	40	8	1	8	11,9	11,9	15:15	15:15
14	PLA	TRILAB	Vertical	60	8	1	8	11,9	11,9	15:15	15:15
15	PLA	Prusa	45°	20	1	5	5	29,3	146,5	4:39	23:15
16	PETG	Prusa	45°	20	1	5	5	29,3	146,5	4:39	23:15
17	PETG	Prusa	Horizontal	60	1	5	5	13,4	66,9	1:58	9:50
18	PETG	TRILAB	Horizontal	60	1	5	5	13,4	66,9	1:58	9:50
19	PETG	Prusa	Vertical	5	1	5	5	15,8	78,8	2:34	12:50
20	PETG	Prusa	Vertical	60	11	1	11	173,3	173,3	32:05	20:54
21	PETG	TRILAB	Vertical	5	1	5	5	15,8	78,8	2:28	12:20
22	PETG	TRILAB	Vertical	60	11	1	11	173,3	173,3	30:16	30:16
						Total:	142	Total [g]:	1331	Total [h]:	314:12

To obtain comparative data for comparing different printers and materials, as well as benchmark material properties for use in the numerical model, the first set of tests was conducted on horizontally oriented specimens in accordance with ISO 527-2, using test sample type 1A [16]. These tests serve as a foundation for assessing the mechanical properties across different setups and materials, ensuring consistency for later stages of numerical modeling and analysis.

To evaluate IFBS, tests were conducted on vertically printed specimens, where all layers are aligned vertically on top of each other. Conducting tensile tests on these specimens allows for the measurement of the tensile strength of the IFBS, or the "glue" strength between the layers.

To gather data on how layer time affects material properties, the number of specimens printed simultaneously was varied. Increasing the number of specimens proportionally increases the time required to print a single layer, leading to variations in the temperature of the last printed layer before the next one is applied. This temperature variation is hypothesized to influence the bonding strength between layers. This paper aims to test this theory and quantify how layer time impacts the strength of 3D-printed parts.

3.3 Testing procedure

As there is yet no specific standard for testing additive manufactured FDM's, whole experiment is based onto testing procedure and conditions given by ISO 527. That and ANSI D638 [21] are most prevalent in scientific papers. They both address the same subject matter but differ in technical content. ISO 527-2 [16] outlines the specific test conditions for assessing the tensile properties of molding and extrusion plastics, following the general principles established in ISO 527-1. This standard provides a framework for consistent and reliable determination of tensile behavior in these materials [9].

3.3.1 Stress – strain curve

The mechanical properties of materials are critical in determining their behavior under applied loads. The elastic modulus is a fundamental property that governs the degree of deformation a material experiences under stress, while the material's strength defines the maximum stress it can endure before failure. Additionally, ductility is a key factor in assessing a material's capacity to withstand deformation beyond its elastic limit without fracturing. Given that all mechanical systems are subjected to various loads during their operational lifespan, it is essential to comprehend the behavior of the materials constituting these systems. Understanding these properties is crucial for the design and analysis of safe and efficient mechanical structures [22].

Tensile test is conducted on a specimen to get the connection between stress and strain. Tensile axial force is gradually applied to the specimen, and the resulting deflection is being recorded as the force increases. These measurements are typically plotted as a load-deflection curve. The deflection of the specimen depends on both the elastic modulus of the material and the specimen's geometry

(such as its cross-sectional area and length). To study the material's intrinsic properties without the influence of its geometry, the data is often generalized to eliminate geometric effects. This is accomplished by transforming the load into stress values and the deflection into strain values [23].

Stress:

$$\sigma = \frac{F}{A} \tag{3.1}$$

where is:

σ stress [MPa]

F force applied [N]

A the original cross-sectional area of the test specimen [mm^2]

Strain:

$$\varepsilon = \frac{\Delta L_0}{L_0} \tag{3.2}$$

where is:

ε strain [Ø]

L_0 is the gauge length of the test specimen [mm];

ΔL_0 is the increase of the specimen length between the gauge marks [mm].

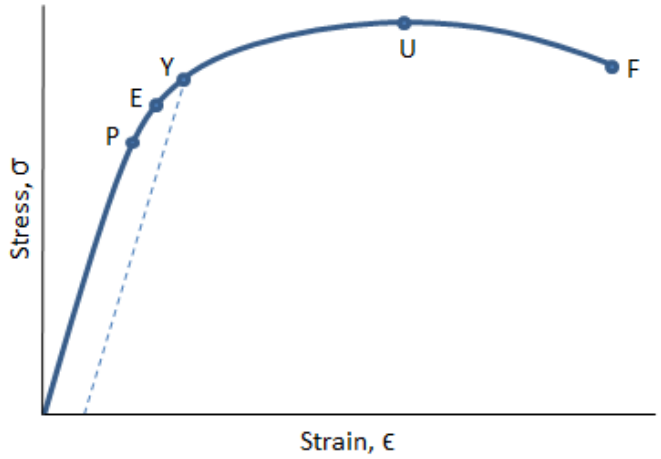

Figure 3.7. Stress-Strain curve with typical points [22]

The stress-strain curve, illustrated in Figure 3.7., is derived from tensile test data. It is a fundamental tool for understanding the mechanical properties of materials. Several critical points on this curve are of particular interest:

Proportionality Limit (P) - the highest stress at which the stress-strain curve remains linear. The slope of this linear segment corresponds to the elastic modulus; E, also known as Young's modulus or the modulus of elasticity. Within this region, Hooke's law applies, describing the relationship between stress and strain over the elastic modulus:

$$\sigma = E \cdot \varepsilon \tag{3.3}$$

where is:

E Young’s modulus of elasticity [GPa]

Elastic Limit (E) - the maximum stress that a material can endure and still return to its original shape upon unloading, without any lasting deformation. Even though the curve may deviate from linearity between the proportionality limit and the elastic limit, the material's behavior is still elastic. If the applied load is removed at or below this limit, the specimen will revert to its original dimensions.

Yield Point (Y) - marks the stress level at which plastic deformation begins, resulting in a significant increase in strain with little additional stress. The stress at this point is known as the yield strength, σ_y. For materials without a well-defined yield point, the 0.2% offset method is often used. This involves drawing a line parallel to the initial linear portion of the curve that intersects the strain axis at 0,002. The point where this line meets the stress-strain curve is defined as the yield point.

Ultimate Tensile Strength (U) – marked as σ_m , represents the maximum stress observed on the stress-strain curve, also referred to as tensile strength. After reaching this point, ductile materials typically exhibit necking, which is characterized by a localized reduction in the cross-sectional area.

Fracture Point (F) – or break point, is where the material ultimately fails and separates into two distinct pieces [3].

After a material yields, it undergoes substantial plastic deformation. During this stage, strain hardening occurs, leading to an increase in the material's strength. As shown in the stress-strain curves in Figure 3.8., there is a noticeable increase in strength between the yield point and the ultimate strength, which is due to the strain hardening process [22].

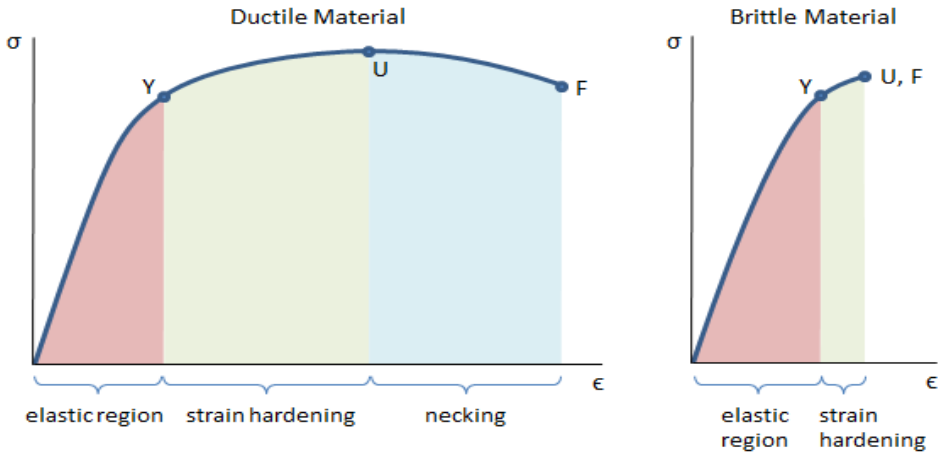

Figure 3.8. Typical Stress-strain diagram of ductile and brittle material [22]

For ductile materials, as illustrated in Figure 3.8., the specimen is capable of carrying additional load even after reaching the ultimate strength. However, beyond this point (U), the increase in strength due to strain hardening is outweighed by a reduction in load-bearing capacity, primarily caused by a reduction in the cross-sectional area. Between the ultimate strength and the fracture point, the engineering stress of the material decreases, and necking is observed [22]. Tensile testing results indicate that horizontally printed specimens display this behavior.

Conversely, the stress-strain curve for brittle materials in Figure 3.8. shows only a small region of strain hardening between the yield point and ultimate strength. It is crucial to note that brittle materials may not exhibit significant yielding or strain hardening; instead, failure often occurs along the linear portion of the curve without substantial plastic deformation [22]. Vertically printed test specimens exhibit a similar stress-strain behavior.

3.3.2 Printing parameters

Starting condition of this part is to find set of parameters that works well on both printers. Preliminary tests consisting of 9 test print series per printer were conducted. Build orientation as well as printing parameters were variated. Each variable was varied independently, and the tensile strength was measured. Insights of these preliminary test results provided the settings for specimens in the testing phase. The specimen had no infill and was consisted completely of perimeters. Brim was used on vertical to increase bed adhesion and support material was used on horizontal and 45° one.

Other parameters are shown in Table 3.3. Both printers have most commonly used 0,4 mm nozzle. Their default layer height is 0,2 mm. Extrusion width of 0,4 mm emerged from fact that specimen is 4 mm thick which makes it even 10 layers wide. Print speed was determined as highest possible that still ensures equal quality of print throughout all layers. Limiting factor here was case with Prusa and vertically oriented specimen. That was most unstable scenario. PETG one even had to have support. Nozzle and bed temperatures was taken from manufacturer of filament requirements [10] [11].

Table 3.3. Constant printer parameters

Parameter	Value	Unit
Layer height	0,2	mm
Extrusion width	0,4	mm
Print speed	20	mm/s
First layer speed	15	mm/s
Travel speed	50	mm/s
PLA nozzle temperature	210	°C
PLA bed temperature	60	°C
PETG nozzle temperature	250	°C
PETG bed temperature	90	°C

Only variation between printer's parameters were in first layer. Nozzle temperature was different because there was problem with low bed adhesion on AzteQ when using same first layer settings as on Prusa. That was mostly because of AzteQ being less directly positioned in a room in relation to A/C and it has a chamber that even left open still affects chamber temperature. Also, AzteQ has extruder mounted far away from nozzle what makes it less able to force filament outside it's ideal working conditions. That caused extruder gear skipping because of '*heat creep'* of filament at default temperature. *Heat creep* refers to the phenomenon of unsteady heat transfer within the hot end of a 3D printer, leading to premature melting of the filament outside the intended melt zone. This premature melting can cause clogs within certain components of the printer, particularly along the extrusion path and within the thermal barrier tube [24]. Consistent prints on AzteQ were achieved with first layer nozzle temperature for PLA of 190 °C. Prusa had opposite problem, and its nozzle temperature were increased to 220 °C. PLA was printed on AzteQ with door open, and PETG with door closed. That made chamber temperature over 40 °C.

3.3.3 Post processing of test specimens

All surfaces of the test specimen were checked visually to be free from visible flaws, scratches or other imperfections. Dimensions were checked with calibrated micrometer. Most importantly, values for width and thickness of each specimen at the centre of the specimen and within 5 mm of each end of the gauge length were checked and made sure that they are within the tolerances indicated in Table 3.3. A lot of specimens showing observed departure from acceptable standard of well printed specimens were rejected. On the other hand, all specimens that passed visual inspection also were inside given tolerances. The test specimens were conditioned for at least 16h before tensile test, as specified in the standard. Atmosphere were regulated to 23 ± 2 °C thorough whole process [16].

All printed specimens were tested on UTM. After examining all measured data, initial table and stress-strain graph were made. That info was used to judge measurements on a specimen-by-specimen case. Mostly data was adequate and in line with what's expected. Measured data was compared with each other and they all together with filament manufactured data [9] and other research papers [25]. This way, few outliers were found that were excluded from further data analysis and reprinted again. Next reason to discard a specimen is if it broke outside of measuring range (Figure 3.9. specimen 3). Also, there were parts that had slight curve on a line between zero and yield point, that resulted in much smaller calculated modulus of elasticity. Lastly there were specimens where all calculated data seemed adequate but when stress-strain diagram were plotted, it was obvious that there was problem with, most likely, kind of extensometer slippage (Figure 3.9. specimen 2).

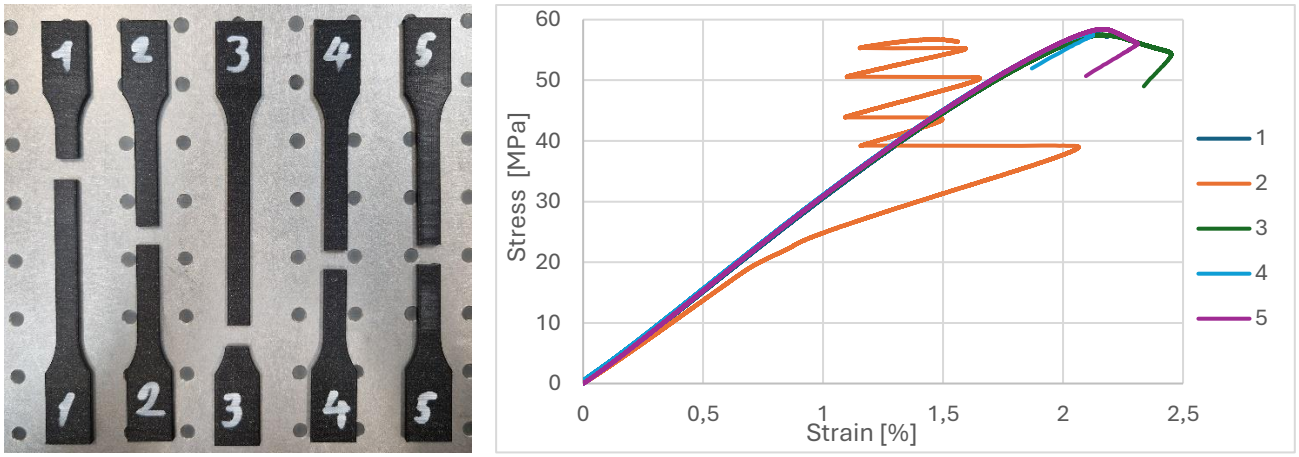

Figure 3.9. Series 6 – Horizontally printed specimens on AzteQ; test specimens (left), corresponding stress-strain plot (right)

3.3.4 Tensile testing

The test specimen is mounted on UTM grips. Where it is extended along its major longitudinal axis at a constant speed until the specimen fractures or until the stress (load) or the strain (elongation) reaches predetermined value. In this case that was insured by break detection. When system detects large dip in stress it means specimen has broken. During this procedure, the load sustained by the specimen and the elongation are measured [16]. Figure 3.10. left shows how verticality of specimen placing was insured. Figure 3.10. middle shows grippers at its home position; at distance of 115 mm. Little helper plate mounted on right side of both grippers mark position where vertical axis of the test specimen are aligned with the axis of the testing machine, as well that it is mounted in the middle of grippers horizontally and vertically. On right is shown test sample with mounted extensometer after fracturing.

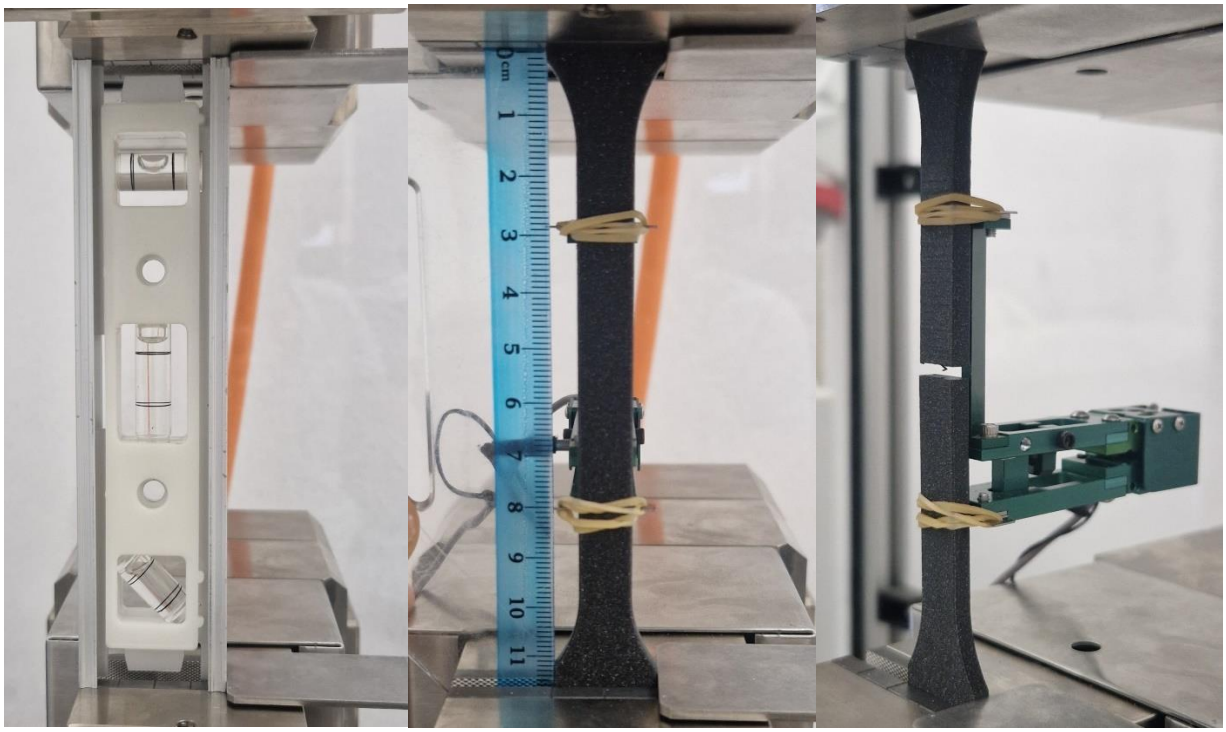

Figure 3.10. Mounting verticality guides (Left), mounted test sample (middle), end of test (right)

The grips were tightened one at a time to ensure even and secure hold on the test specimen, which is crucial for preventing any slippage of the specimen or unintended movement of the grips during the

testing process. This careful approach helps maintain accurate alignment and consistent tension, which are essential for reliable test results. When mounting the test specimens, it is possible to introduce some residual prestresses. These prestresses often arise from the pressure exerted by the grips, especially in materials that are less rigid. Despite seeming undesirable, these prestresses play a vital role in eliminating a "toe region" at the start of the stress-strain curve, which can otherwise cause inaccuracies in the initial linear portion of the graph [6].

A minimum of five test specimens were tested for each testing series, as required. Dumbbell-shaped specimens that broke or slipped within the grips were excluded from the analysis, and additional specimens were printed and tested to replace them. However, data showing variability were not excluded, as such variability reflects the inherent nature of the material being tested [9].

3.4 Metallographic analysis

Metallographic analysis helps in understanding the quality of the print, the integrity of the bonds between layers, and the presence of any defects or anisotropies specific to the additive manufacturing process [26]. Here it's made also to get insights into inside gap sizes of specimens. Surfaces where the fracture occurred in tensile testing are examined under a microscope.

On Figures 3.11. & 3.12. are shown pictures taken with digital microscopic camera *Dino-Lite AM7013MZT* [27] and processed with software *DinoCapture 2.0*. Figure 3.11. shows metallographic cut of specimen from series 1., horizontally single printed PLA sample on Prusa.

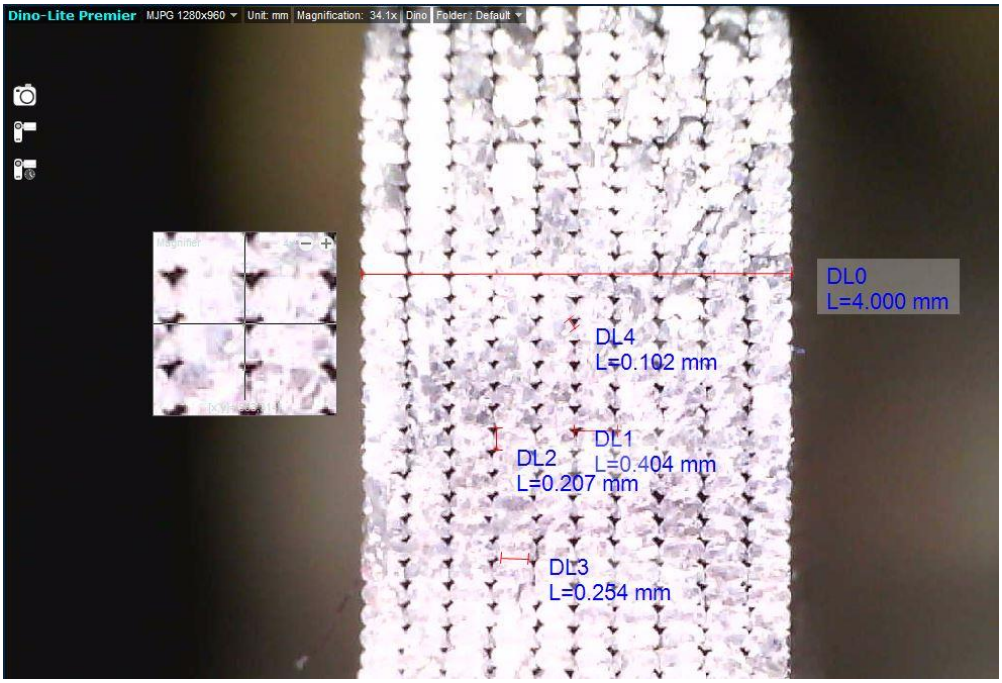

Figure 3.11. Metallographic cut of horizontal test specimen

Figure 3.12. shows series 21 vertical single printed PETG specimen on AzteQ.

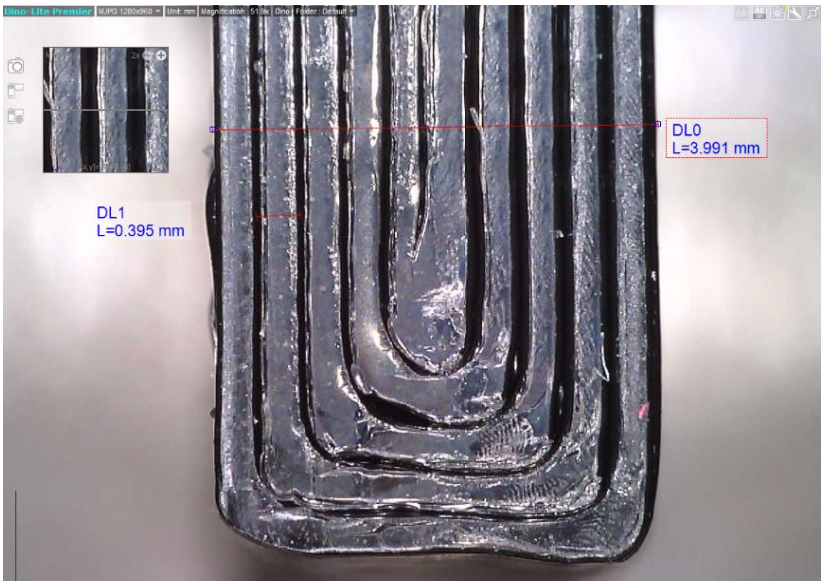

Figure 3.12. Metallographic cut of vertical test specimen

The molten filament is extruded into shape corresponding ellipse or oblong shape. To achieve good bond between surrounding perimeters, as well as good bond between the layer underneath or the bed, they are made flattened to be interference fit. That makes their shape in end most similar to a rectangular with fillet on its corners. Extruding a perfect circle would make it very weak since each layer would barely be touching each other [28].

Width of test specimen is visible at 4 mm. It is tall 10 mm. Single line of extrusion is defined in slicing software 0,4 width and 0,2 layer height that matches with measured values. That makes its perpendicular section consisted of 10 x 100 matrix of same oblong shape lines. There is variance between line size. Multiple single lines were measured and averaged. Because of gravity, fillets on upper side of extruded lines have bigger radius then those on the bottom. That was taken in considerations and average fillet from all four corners is calculated. Figure 3.13. is shown average dimension of single line that rest of calculations is based on. That data is used to calculate area of specimen and make FEM later in paper.

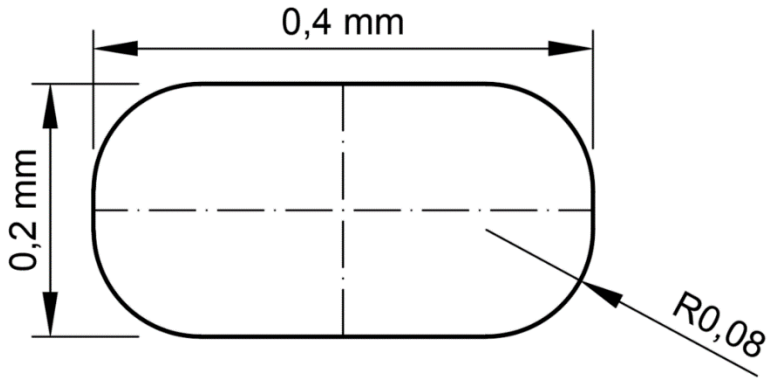

Figure 3.13. Single extruded line dimension

3.4.1 Calculation of adjusted surface

Stress is function of force acting on the surface. Perceived surface of FDM-s is at first homogenous, but even when part is printed only with perimeters there are still gaps left. Gaps between lines (on Figure 3.11. visible as black spots between four extruded lines) are measured to calculate adjusted surface. That surface is then used to calculate stress and over it, modulus of elasticity is more precisely

determined. As seen on Figure 3.14. typical gap is consisted of area that four quarter-circles form. Their radius is r = 0,08 mm.

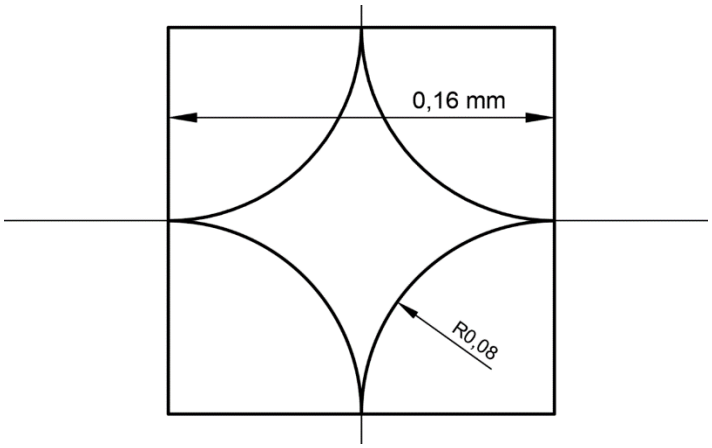

Figure 3.14. Typical gap size

The area of a one quarter-circle is:

$$A_{\frac{1}{4}circle} = \frac{1}{4}\pi r^2 \tag{3.4}$$

Total area of the four quarter-circles is:

$$A_{circle} = 4 \cdot \frac{1}{4}\pi r^2 = \pi r^2 \tag{3.5}$$

The side length of the square is equal to the diameter of the quarter-circle, which is $2r$. Therefore, the area of the square is:

$$A_{square} = (2r)^2 = 4r^2 \tag{3.6}$$

Area of gap:

$$A_{gap} = A_{square} - A_{circle} \tag{3.7}$$

$$A_{gap} = 4r^2 - \pi r^2 = (4 - \pi)\, r^2$$
$$A_{gap} = (4 - \pi)\, 0.08^2 = 0.005504\, mm^2$$

Calculated cross section of a horizontal test specimen consists of a 10 x 100 grid of single lines. Same can be determined empirically from Figure 3.11. Gaps are formed only in places where they are surrounded on all sides by other ellipses. That means that number of gaps is by one less than extruded lines. Therefore, its grid is 9 x 99.
Total adjusted area is calculated as:

$$A_{total} = A_{ideal} - (9 \cdot 99) \cdot A_{gap} \tag{3.8}$$
$$A_{total} = 4\, mm \cdot 10\, mm - (9 \cdot 99) \cdot 0{,}005504\, mm^2$$

$$A_{total} = 35{,}51\, mm^2$$

All results presented in this paper were calculated using the adjusted surface area, with the exception of comparisons made with other studies, where the original cross-sectional area was used for their calculations.

4. TENSILE TESTING RESULTS

This section presents the results of tensile testing. Initially, typical horizontal and vertical cases are examined, which will serve as the basis for establishing the numerical model. The influence of different printers, layer time, and build orientation on the material properties of both tested materials is then analysed, providing insights into how these factors affect the strength and performance of the printed specimens.

Data acquired by UTM are expressed as Load (N) and Strain (%). Strain is automatically converted from mV/V captured by extensometer to distance mm/mm or % with equation (3.2). Stress is determined using the equation (3.1) with value of adjusted area calculated in (3.9).

Altogether 22 series of testing were made consisting of two different materials, two printers, three printing orientation and multiple variations of time per layer. Average values were calculated and shown on Table 4.1., To streamline terminology, the printers will hereafter be referred to as "Prusa" and "AzteQ" for the remainder of this paper.

The maximum recorded force, ultimate tensile strength, and modulus of elasticity were, as expected, observed in horizontally oriented specimens made of PLA. PLA, being more brittle but with higher strength, allowed the horizontally oriented specimens to sustain significantly greater loads before fracturing. Following this, the PETG horizontal specimens demonstrated 300-400 N lower load-bearing capacity across all test series. PLA vertical specimens exhibited approximately half the strength of their horizontally oriented counterparts. The weakest material properties were recorded for PETG vertical specimens, with a fracture occurring at less than 1 kN. These results are further analyzed and presented in detail in the subsequent sections of the chapter.

Table 4.1. Tensile testing results

Series	Material	Printer	Orientation	t_1 [sec]	F_m [N]	ε_m [%]	σ_m [MPa]	σ_y [MPa]	E_t [GPa]
1	PLA	Prusa	Horizontal	60	2303	3,21	64,867	62,580	3,352
2	PLA	Prusa	Horizontal	180	2348	4,14	66,112	62,807	3,127
3	PLA	Prusa	Horizontal	300	2363	3,79	66,535	63,208	3,259
4	PLA	AzteQ	Horizontal	60	2335	2,21	65,746	62,459	3,415
5	PLA	AzteQ	Horizontal	180	2286	2,17	64,388	61,168	3,310
6	PLA	AzteQ	Horizontal	300	2302	2,23	64,879	61,635	3,209
7	PLA	Prusa	Vertical	5	1255	1,42	35,346	35,346	2,454
11	PLA	Prusa	Vertical	20	1063	1,24	29,948	29,948	2,257
13	PLA	Prusa	Vertical	40	1054	1,31	29,734	29,734	2,357
8	PLA	Prusa	Vertical	60	1056	1,33	29,735	29,735	2,470
9	PLA	AzteQ	Vertical	5	1783	1,95	50,205	50,205	2,816
12	PLA	AzteQ	Vertical	20	1646	1,75	46,363	46,363	2,852
14	PLA	AzteQ	Vertical	40	1624	1,81	45,726	45,726	3,046
10	PLA	AzteQ	Vertical	60	1549	1,91	43,619	43,619	2,810
15	PLA	Prusa	45°	20	1068	0,88	30,084	30,084	3,029
16	PETG	Prusa	45°	20	788	0,77	22,178	22,178	2,192
17	PETG	Prusa	Horizontal	60	1799	0,95	50,673	48,140	2,203
18	PETG	AzteQ	Horizontal	60	2022	0,75	56,950	54,102	2,019
19	PETG	Prusa	Vertical	5	446,09	0,51	12,56	12,562	2,12
20	PETG	Prusa	Vertical	60	222,16	0,30	6,26	6,256	1,87
21	PETG	AzteQ	Vertical	5	781,61	0,67	22,01	22,011	2,70
22	PETG	AzteQ	Vertical	60	626,00	0,68	17,63	17,629	2,69

Calculated values are as following:

t_1 Time per one layer (used to determine IFBS) [sec];

F_m Load at ultimate strength [N];

σ_m Ultimate strength - stress at the first local maximum observed during a tensile test [MPa];

ε_m Strain at strength - strain at which the strength is reached [mm/mm] or [%];

σ_y Tensile yield strength – expressed sometimes as $\sigma_{0.2}$ (It may be less than the maximum attainable stress [MPa];

ε_y Strain at tensile yield strength - strain at which the tensile yield strength is reached [mm/mm] or [%];

E_t The tensile modulus is defined as the ratio of tensile stress (force per unit area) to strain (relative deformation) in a material when it undergoes elastic deformation. [GPa].

The ultimate tensile strength is defined as the stress at the first local maximum observed during a tensile test. For certain materials, such as plastics, this stress may correspond to either the point at which the specimen yields or the point at which it breaks. In horizontally printed specimens, this occurred at the yield point, whereas in vertically printed specimens, it occurred at the break point. The tensile modulus is calculated as the slope of the stress-strain curve, $\sigma(\varepsilon)$, within the strain range from $\varepsilon_1 = 0{,}05\ \%$ to $\varepsilon_2 = 0{,}25\ \%$ [9]. For specimens exhibiting a toe region at the beginning of the stress-strain curve, the slope was measured after a specified radius, while remaining within the linear region.

The determination of strain values using an extensometer involves averaging strain over the gauge length of the specimen. This method is accurate and effective as long as the deformation within the gauge length is homogeneous. However, if the material begins to neck, as observed in the horizontal PETG cases, the strain distribution becomes inhomogeneous. In such instances, strain measurements obtained with an extensometer are significantly affected by the position and size of the necking zone. To accurately present stress-strain evolution on a graph in these cases, motor position (measured in mm) is utilized instead of strain.

4.1 Determining material properties for numerical model

In this section, the data required for developing the numerical model will be presented. Horizontal specimens are analysed to model the printed layers as isotropic material, while vertical specimens are used to determine the IFBS between layers. This distinction is critical for accurately representing the material behaviour in the numerical model, with horizontal specimens capturing uniform properties and vertical specimens highlighting the effects of layer adhesion.

In Figure 4.1, stress-strain plots of the tested specimens are presented. A clear similarity can be observed among specimens printed on the same printer. All specimens exhibit a maximum stress of under 70 MPa. The average strain values are 3.3% for specimens printed on the Prusa printer and 2.1% for those printed on the AzteQ printer, highlighting the variation in material behavior based on the different setups used for printing.

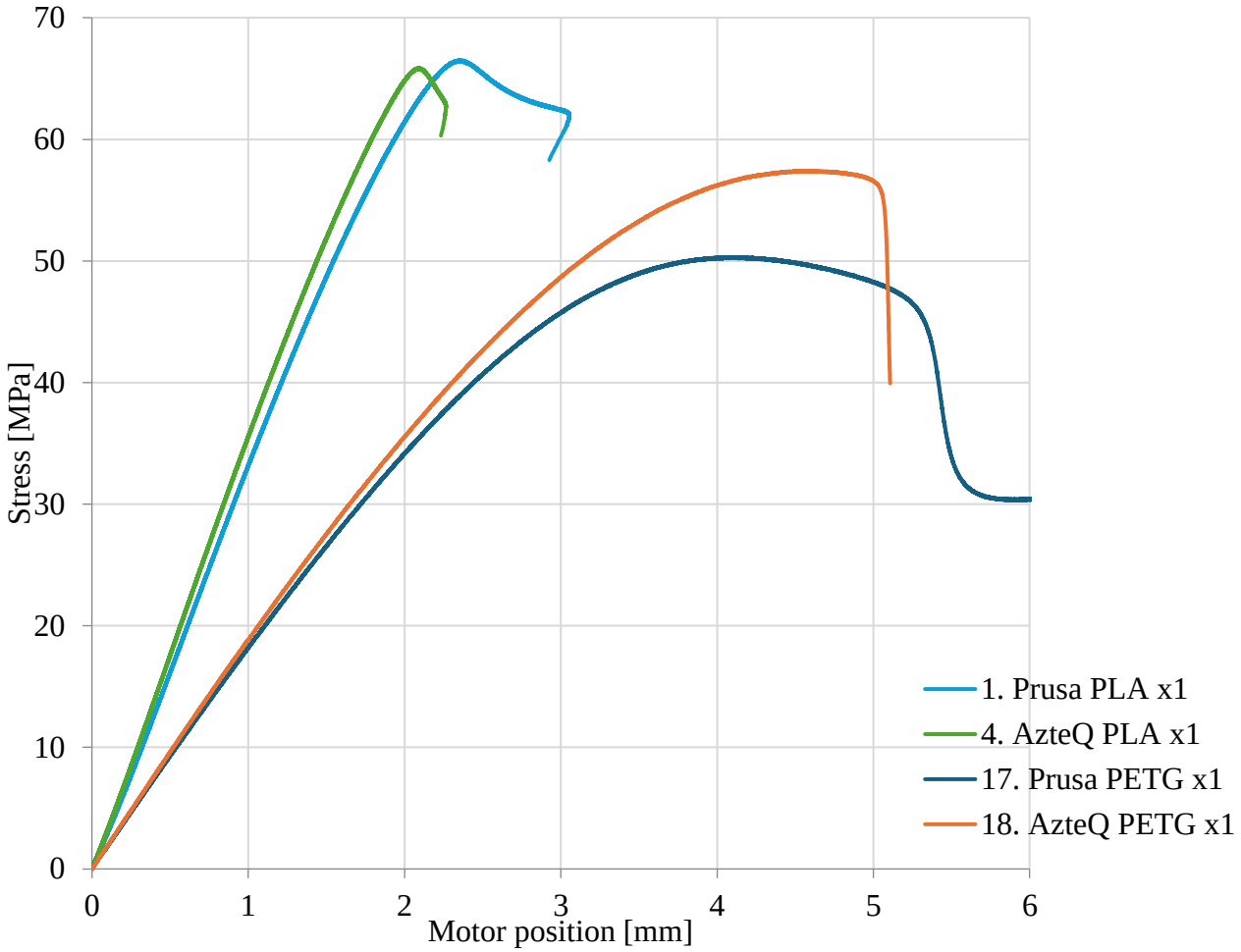

Figure 4.1. Stress–strain plot – Horizontally oriented specimens

Figure 4.2 shows the stress-strain plots for vertically oriented PLA specimens. A similar differentiation between the two printers is evident, as seen with the horizontal specimens. Variability in the ultimate strength achieved is apparent in the vertically oriented specimens. The highest stress values were recorded in single-printed specimens for both printers, and a clear correlation exists between the increasing number of specimens printed simultaneously and a decrease in the maximum stress achieved.

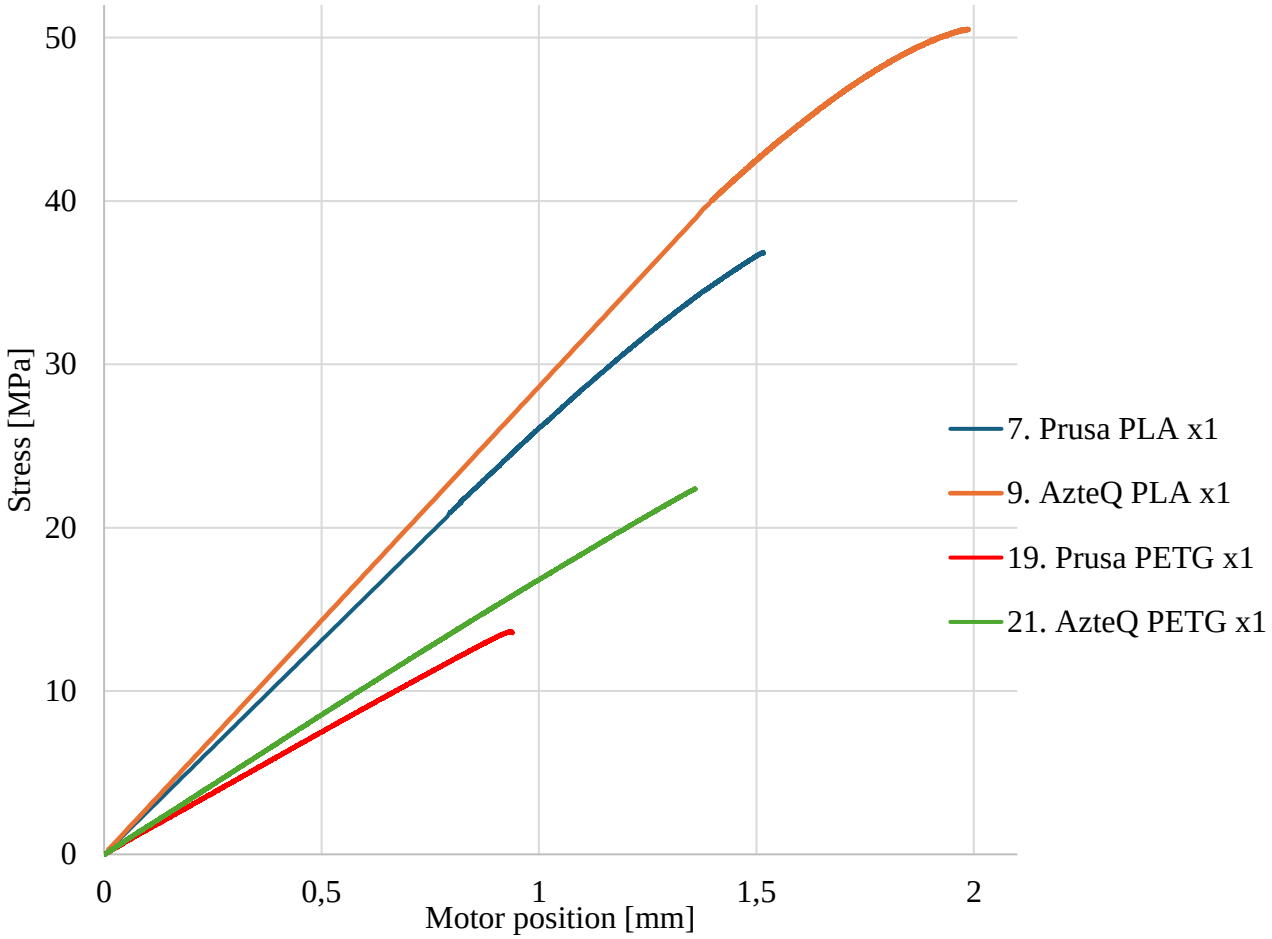

Figure 4.2. Stress–strain plot – Vertically oriented specimens

Table 4.2 presents a comparison of the ultimate stress and elastic modulus values, both for the original cross-section and for the adjusted cross-section with gaps removed. To develop a representative model for finite element analysis (FEM), values from the adjusted cross-sectional area will be used, and for comparison with other studies, the original cross-sectional area of 40 mm². This dual approach ensures both accuracy in numerical modeling and consistency when comparing results with existing literature.

Table 4.2. Comparison of material properties for different cross-section areas

			A =	40 mm^2	35,51 mm^2	40 mm^2	35,51 mm^2
Series	Material	Printer	Orientation	σ_y [MPa]		E_t [GPa]	
1.	PLA	Prusa	Horizontal	55,556	62,580	2,814	3,352
4.	PLA	AzteQ	Horizontal	57,594	62,459	3,105	3,415
7.	PLA	Prusa	Vertical	31,378	35,346	2,231	2,454
9.	PLA	AzteQ	Vertical	44,569	50,205	2,560	2,816
17.	PETG	Prusa	Horizontal	44,985	48,140	2,003	2,203
18.	PETG	AzteQ	Horizontal	50,557	54,102	1,835	2,019
19.	PETG	Prusa	Vertical	11,152	12,562	1,93	2,12
21.	PETG	AzteQ	Vertical	19,540	22,011	2,70	2,7

Comparing our measured results with the manufacturer's data reveals some discrepancies. Table 4.3 provides values from Prusa Polymer's Prusament PLA and PETG. Although the same standard was used for measurement, the tensile modulus for PLA, as provided by Prusament, ranges between 2.3 and 2.4 GPa, whereas our measurements varied from 2.2 to over 3 GPa. The most significant difference was found in the tensile yield strength. In our tests, horizontally oriented PLA specimens achieved approximately 56 MPa, and vertical specimens about 40 MPa. However, Prusament's data shows lower tensile strength for horizontal specimens (51 MPa) and higher for vertical ones (59 MPa).

That trend is opposite of expected for reasons that in horizontal case all filaments participate in load bearing, while at vertical it’s only small area of melted two layers. Similar trends have been observed in other research studies [29], reinforcing our findings.

Table 4.3. Mechanical properties of materials tested by manufacturer [10] [11]

	Property/Print Direction	Horizontal	Vertical xz	Unit	Method
PLA	σ_y	51± 3	59 ± 2	MPa	ISO 527-1
	E_t	2,3 ± 0,1	2,4 ± 0,1	GPa	
	ε_y	2,9 ± 0,3	3,2 ± 1,0	%	
PETG	σ_y	39 ± 2	42 ± 1	MPa	ISO 527-1
	E_t	1,7 ± 0,1	1,8 ± 0,1	GPa	
	ε_y	3,5 ± 0,2	3,7 ± 0,1	%	

Prusa material research doesn't state all parameters being used for printing test specimens. Temperature of nozzle and bed are similar. Printing speed, infill and other parameters could be significantly different [10] [11]. This confirms state from numerous research papers that state that because of missing exact standard for AM FDM and its complex nature as anisotropic material is practically impossible to compare values made by different research [25] [30].

Comparative results were found in similar study; "Mechanical properties of components fabricated with open-source 3-D printers under realistic environmental conditions" by B.M. Tymrak et al. [31]. It examines the fundamental tensile strength and elastic modulus of 3D-printed components produced using open-source 3D printers, simulating conditions typical for standard users. For PLA material their findings are in line with ours; the average tensile strength or horizontal specimen is 56.6 MPa, and the average elastic modulus is 3.168 GPa.

4.2 Impact of additive manufacturing devices on the mechanical properties of materials

This section examines the impact of additive manufacturing devices on the mechanical properties of materials. Upon examining the charts in Figure 4.3., there is a noticeable increase in load and stress on parts manufactured using the AzteQ printer, with the most significant differences observed in vertically oriented samples. This trend is consistent across both materials tested. PLA was printed on the AzteQ with the door open, while PETG was printed with the door closed.

For horizontally oriented specimens, there was no variation in strength between the printers when using PLA. However, with PETG, the AzteQ printer achieved a 10 % higher load and ultimate

strength. This difference can likely be attributed to the closed chamber of the AzteQ during the PETG print, suggesting that temperature control played a role in enhancing strength.

A similar pattern is observed with vertical specimens, where the Prusa printer consistently recorded lower strengths for both materials, resulting in lower IFBS values. Since all printing parameters were identical for PLA, the significantly higher values obtained with the AzteQ printer indicate a superior print quality, likely due to the AzteQ's advanced design and features. The Prusa printer, equipped with a Cartesian motion system, contrasts with the AzteQ's fixed build platform, Delta kinematic system, and enclosed chamber. The increased flexibility of PETG exacerbates unwanted movements in the Prusa machine during printing, where the extruder and build platform move in opposite directions, causing specimen flex and negatively impacting print quality, as evidenced by the measured data.

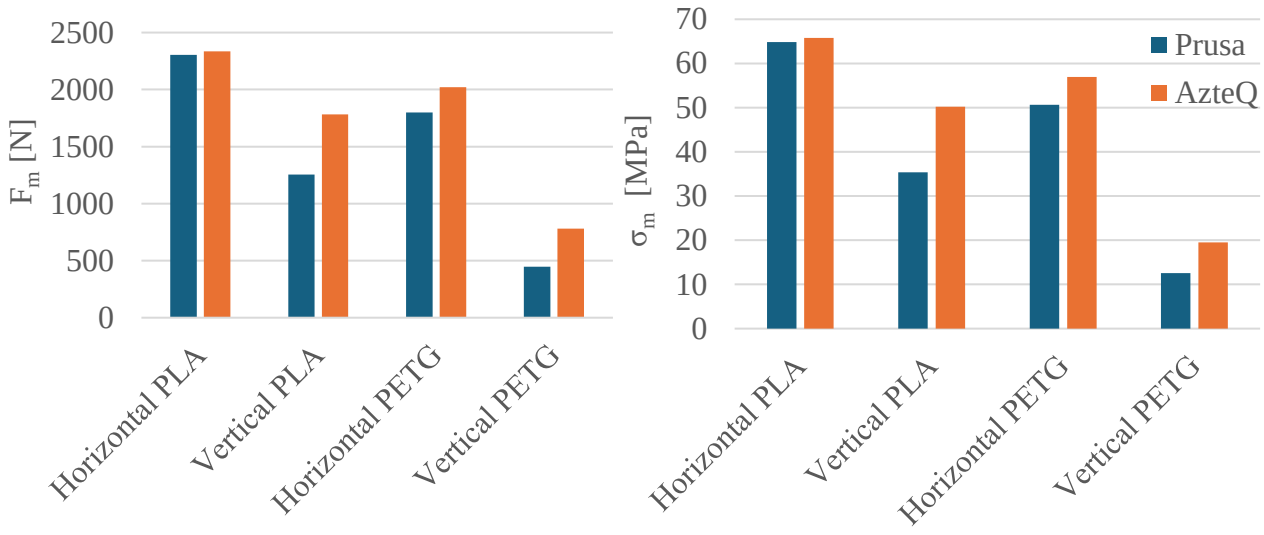

Figure 4.3. Ultimate strength load chart (left), ultimate strength (right) charts

As shown in Figure 4.4, no significant difference was observed in the modulus of elasticity between the printers. The variances were within acceptable tolerances. For horizontally printed PLA samples, lower strain was detected at the same stress level, whereas this trend did not hold for vertically printed specimens. A similar pattern was observed with PETG. Based on Young's modulus measurements, no substantial conclusions regarding printer performance could be drawn.

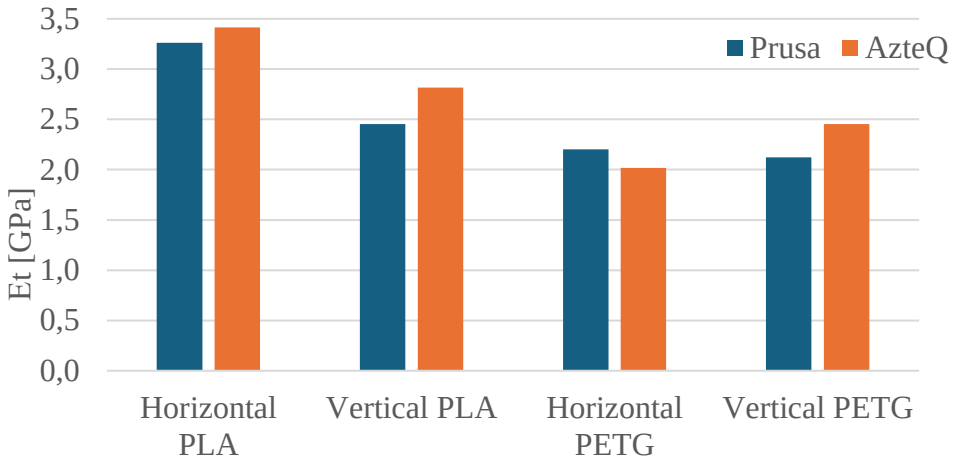

Figure 4.4. Modulus of Elasticity chart

The stress-strain curves align with previously shown charts. Figure 4.5. presents the stress-strain curves for PLA specimens printed in two main orientations on both tested printers. The Prusa printer exhibited a higher strain-to-stress ratio for horizontally oriented PLA specimens at the same ultimate strength. On the other hand, vertically printed PLA specimens demonstrated superior material properties when tested on the AzteQ, showing over 30% higher stress and strain before fracture. This highlights the importance of interfacial bonding strength (IFBS), with the AzteQ outperforming the Prusa in this category.

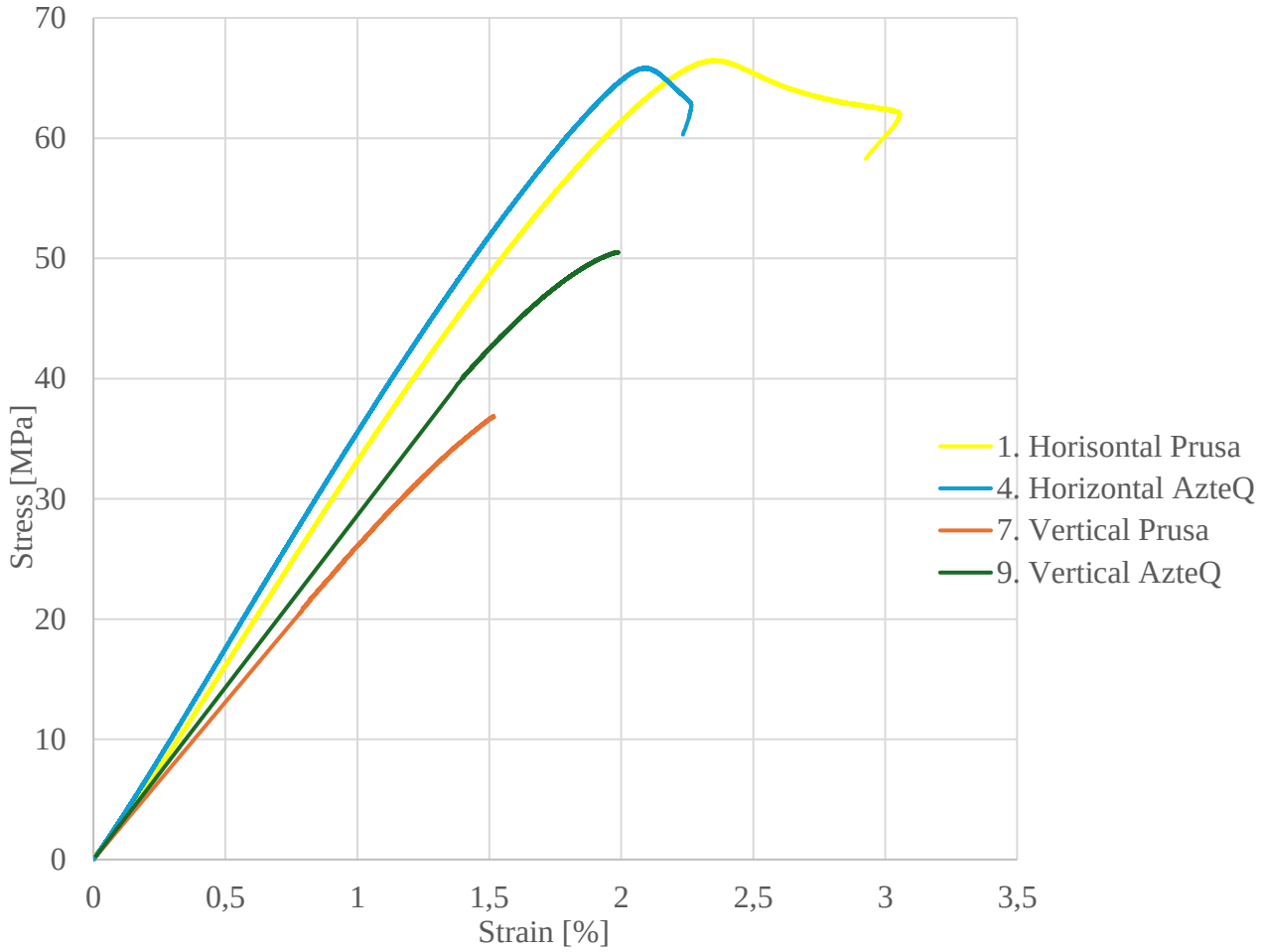

Figure 4.5. Stress–strain plot – PLA specimens

PETG performs better at higher temperatures, and as seen in Figure 4.6, both vertically and horizontally printed specimens exhibit superior material properties when printed on the AzteQ printer. This is likely due to the fact that AzteQ's enclosed chamber maintains a temperature over 20°C above room temperature, which enhances the performance of PETG during printing.

In both orientations, the AzteQ produced stronger parts compared to the Prusa. That difference is probably enlarged because Prusa reached its limits with it's Cartesian motor system. To be able to finish print, both printers vertical PETG specimens were printed with supports.

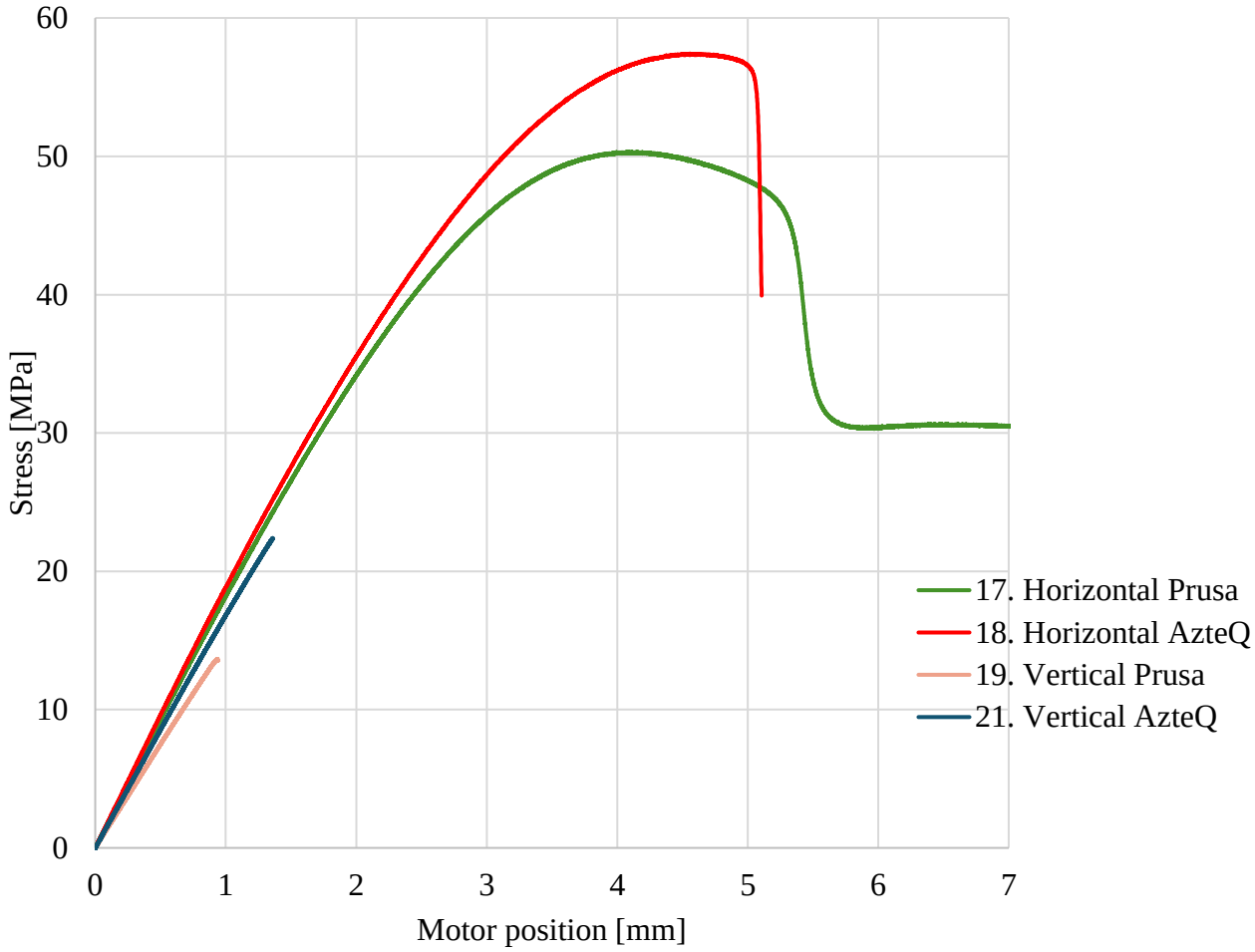

Figure 4.6. Stress–strain plot – PETG specimens

Based on the results, it can be concluded that the Trilab AzteQ Industrial outperforms the Prusa MK3S. Two critical factors contributed to this outcome: the presence of a heated chamber and the Delta kinematic system in the AzteQ printer. The temperature difference provided by the chamber likely had a significant influence on the PETG results. Since horizontal specimens are generally easier to print than vertical ones, the limitations of the Prusa printer did not greatly affect the results for PLA. However, the Delta kinematic system of the AzteQ proved superior for producing narrow vertical prints, giving it an advantage in those cases.

4.3 Impact of the layer time on sample strength

Analysis of the impact of number of simultaneously printed samples on their strength with regard to interlayer bonds in this paper is shortly called as factor layer time. Number of simultaneously printed specimen directly coincides to layer time.

It was always speculated, but until now had no data to confirm next assumption; "Increasing layer time leads to weaker 3D printed parts". When the time needed to print a single layer is varied, it results in a variation in the temperature of the last layer on which the next one is applied. That temperature difference is expected to affect bonding strength between layers.

This experiment involved varying the number of specimens printed simultaneously. For horizontally printed specimens, the quantity ranged from one to three, and finally, five specimens at a time. This caused the layer time to increase fivefold, from 1 minute to 5 minutes. No noticeable difference in material properties was observed, so these results were excluded from the graphs. For vertically printed specimens, the number ranged from one, with a layer time slightly over 5 seconds, to 11 specimens, increasing the layer time to 1 minute. In this case, the data showed a clear downward correlation between increasing layer time and lower values of ultimate strength and load (Figure 4.7.). The data presented is from the AzteQ printer, though a similar trend was noted with the Prusa printer as well.

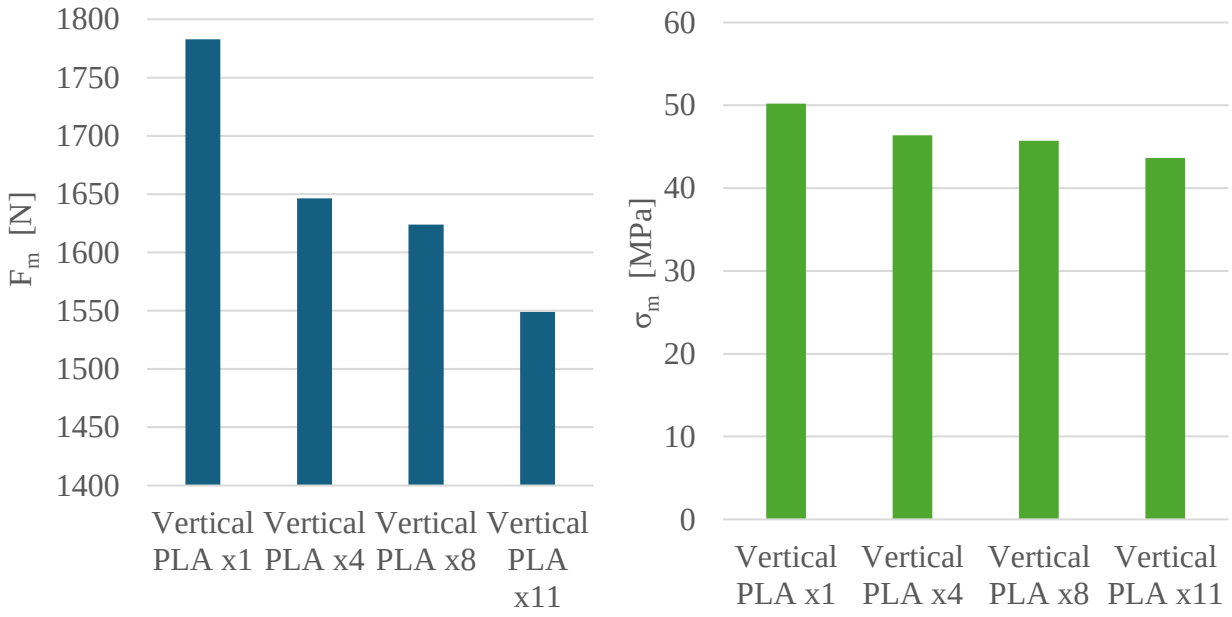

Figure 4.7. Ultimate strength load (left), ultimate strength (right) of AzteQ specimens' chart

Figure 4.8. illustrates the modulus of elasticity for the parts previously discussed. The variations between the series are minimal, making it challenging to draw any definitive conclusions. At horizontal specimen's tensile modulus seems to fall when layer time is increased and at vertical it seems like it stays the same. Increasing number of tested specimens would help here to get significant conclusion.

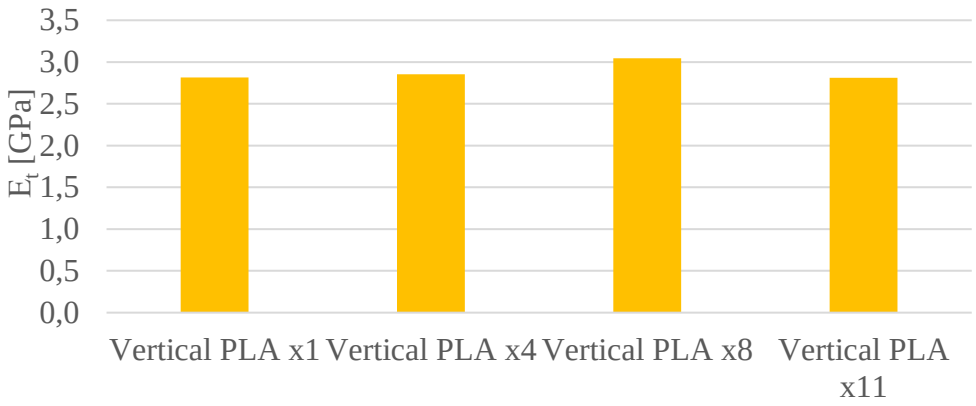

Figure 4.8. Modulus of elasticity of AzteQ specimens' chart

Figure 4.9 presents stress-strain curves for specimens printed on the same printer using the same material, with orientation and layer time being the only variables. For horizontally printed specimens, the curves mostly overlap in the elastic region, differing primarily at the fracture point. In contrast, vertically printed specimens follow a similar pattern initially but break at lower stress values compared to their horizontal counterparts. Additionally, a noticeable trend can be observed in vertically oriented samples: as the number of simultaneously printed specimens decreases, the recorded maximum stress increases.

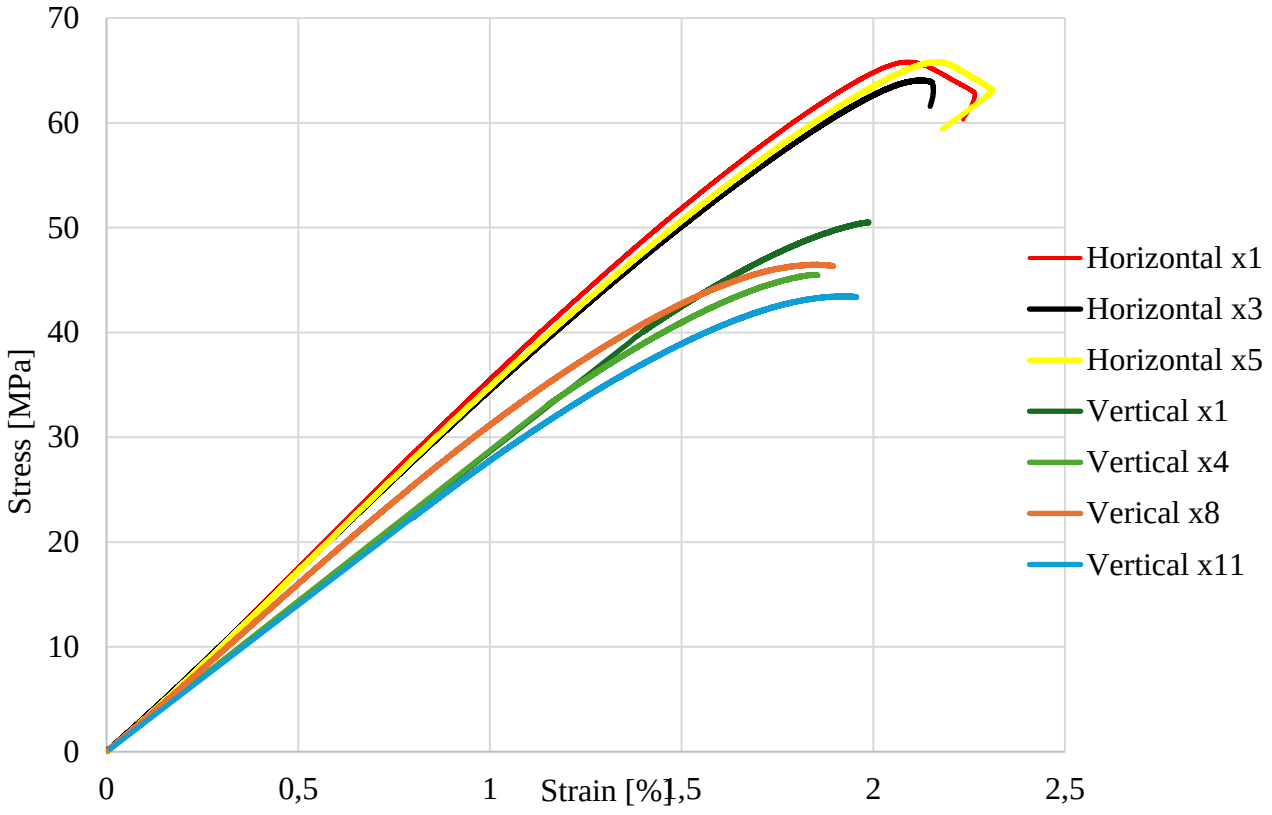

Figure 4.9. Stress–strain plot – AzteQ PLA specimens

A similar trend is observed in the PETG vertical samples, as shown in Figure 4.10. Both the AzteQ and Prusa stress-strain curves are almost perfectly described by a line connecting the initial point and the fracture point. The key difference between the two lies in the layer time. For Prusa, at 5 seconds per layer, there was an increase of nearly 5 MPa in stress before fracturing, compared to the specimen printed at 1 minute per layer. This suggests that shorter layer times can positively influence the material's resistance to fracture.

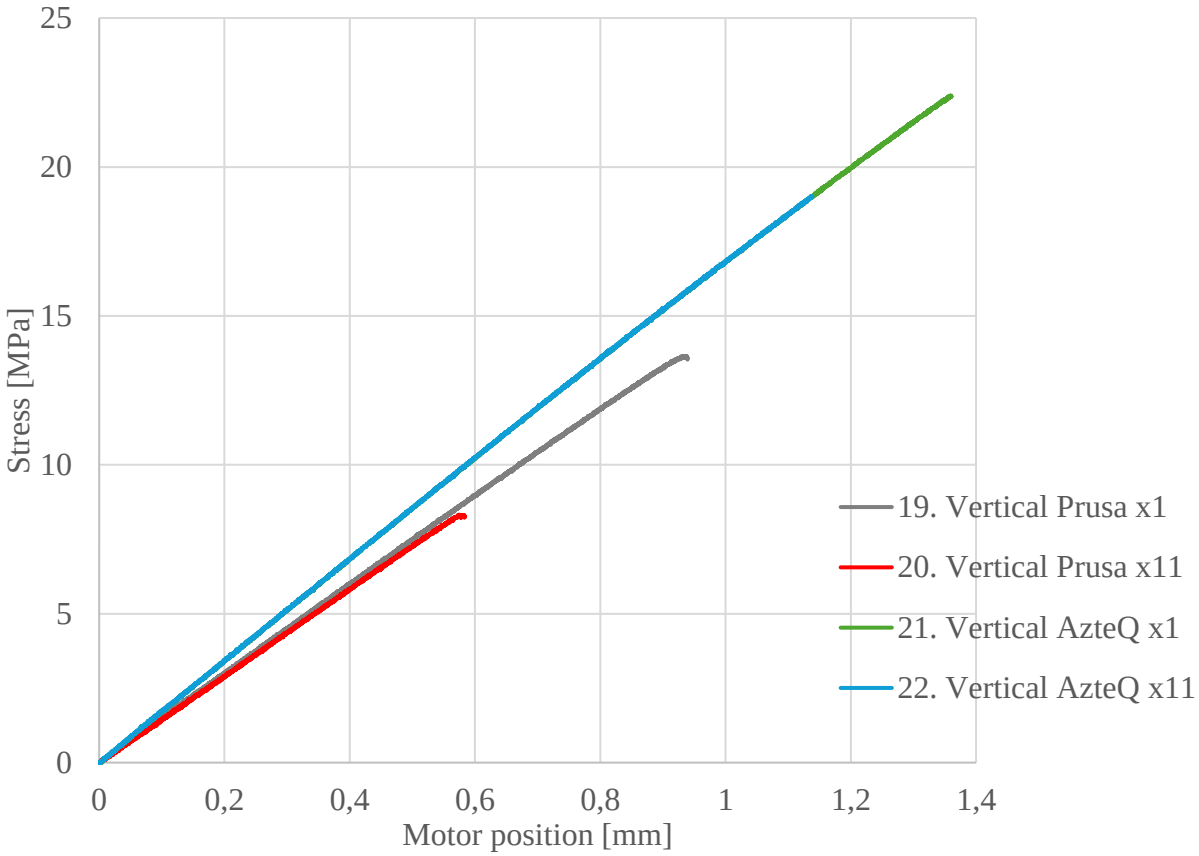

Figure 4.10. Stress–strain plot – Vertical PETG specimens

Horizontally printed specimens have much longer layer times, which is speculated to be the reason why bonding strength between layers is not significantly affected. Despite the layer time being increased fivefold, enough time passed for the last layer to cool down to a similar temperature as previous layers. With the nozzle temperature set at 220 °C, by the time it returns to the same spot, the layer had cooled almost to ambient temperature. In contrast, the layer time for single vertical specimens was only 5 seconds, meaning the last layer remained hot when the next one was applied, which noticeably increased strength compared to multiple vertical specimens.

Since layer time was the only parameter varied, the conclusion is that it definitively affects IFBS. Consequently, for achieving the highest quality prints, it is recommended to print parts individually rather than simultaneously.

4.4 Impact of build orientation on the mechanical properties of materials

Build orientation is one of most widely researched and understood print parameter in scientific papers considering FDM-s. Main difference between horizontal and vertical is in much shorter strain part and as well as lower expected ultimate strength [1] [32].

Orientation, as one of the primary parameters influencing part strength, is clearly reflected in the graphs and charts (Figures 4.11. through 4.16.). All measured parameters show values that are nearly double in horizontally oriented specimens compared to vertically oriented ones. This is expected, as in vertical specimens, only the IFBS holds the layers together, whereas in horizontal specimens, all filaments contribute to load-bearing.

Figure 4.11 displays the maximum load recorded before fracturing, as well as the ultimate strength for both materials, on a Prusa. The same trend is observed across both materials and printers. Horizontal and vertical orientations performed as anticipated, with horizontally oriented specimens showing significantly higher values. The exception is the 45° orientation. In PLA, the 45° oriented specimens consistently fractured at only marginally higher loads than the vertically oriented ones, while PETG exhibited a more expected difference, with 45° specimens performing better than vertical ones but still weaker than horizontal ones.

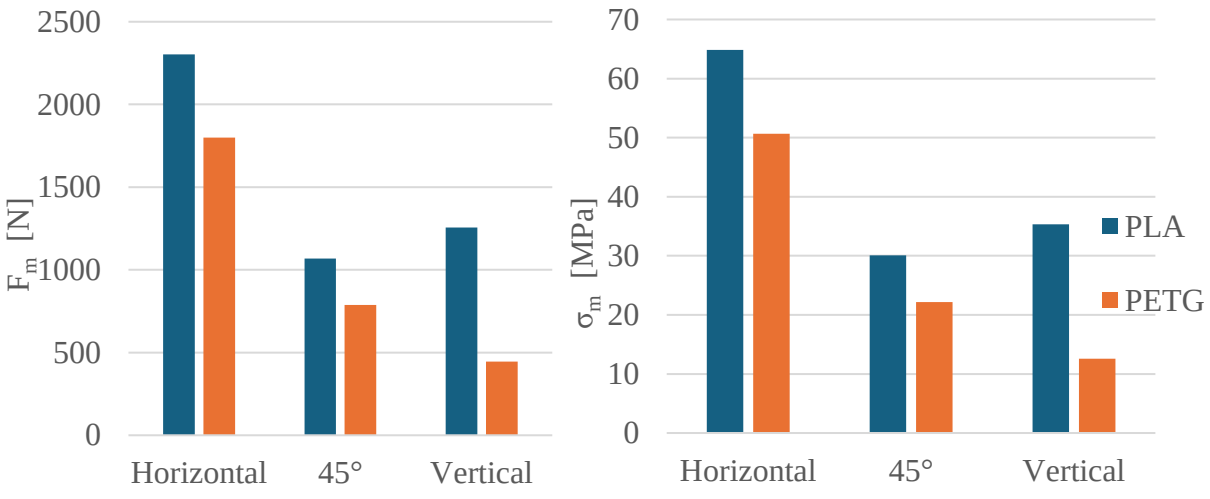

Figure 4.11. Prusa - Ultimate strength load chart (left), ultimate strength (right) chart

Figure 4.12. shows modulus of elasticity between orientations varies only at PLA. PETG having elastic properties, achieve similar Young modulus without regard to build orientation. PLA experiences increasingly lower values when increasing specimen rotation. From 3,3 GPa for horizontal, 3 GPa for 45° and 2,5 GPa for vertical orientation.

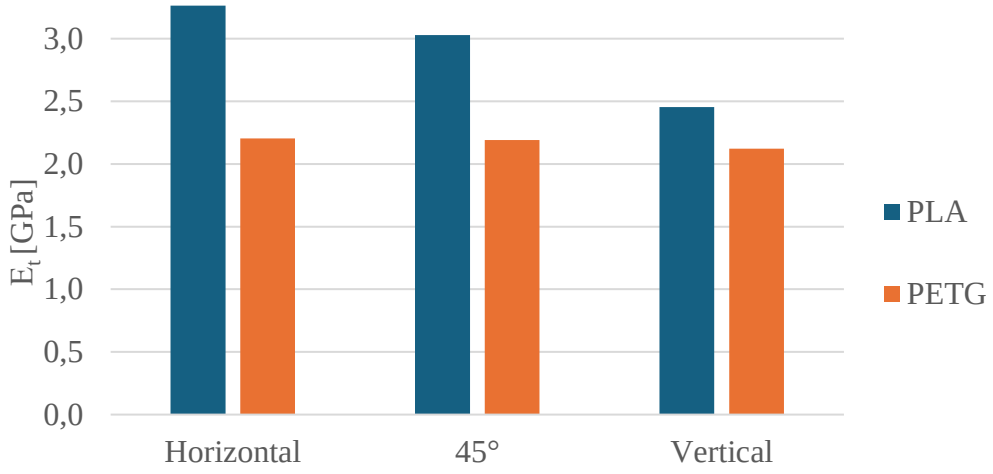

Figure 4.12. Prusa - Modulus of elasticity chart

The stress-strain diagram in Figure 4.13 clearly shows that fractures in vertically oriented specimens occur at lower stress and strain values, behaving like brittle materials with immediate failure and no pronounced yield point. In contrast, the curve for horizontally oriented specimens resembles that of conventional materials, with visible strain hardening followed by the necking region after the yield point. For comparison, strain data was expressed using motor position for PLA in this figure as well.

This serves as a clear example of why part orientation is one of the principal factors affecting mechanical properties. Horizontal specimens exhibit stress values exceeding 40 MPa, while vertical ones fail at under 20 MPa. The vertical specimens were so fragile that one even broke during mounting on the UTM. A bending test would likely reveal an even greater difference in strength between these orientations than the tensile test results indicate.

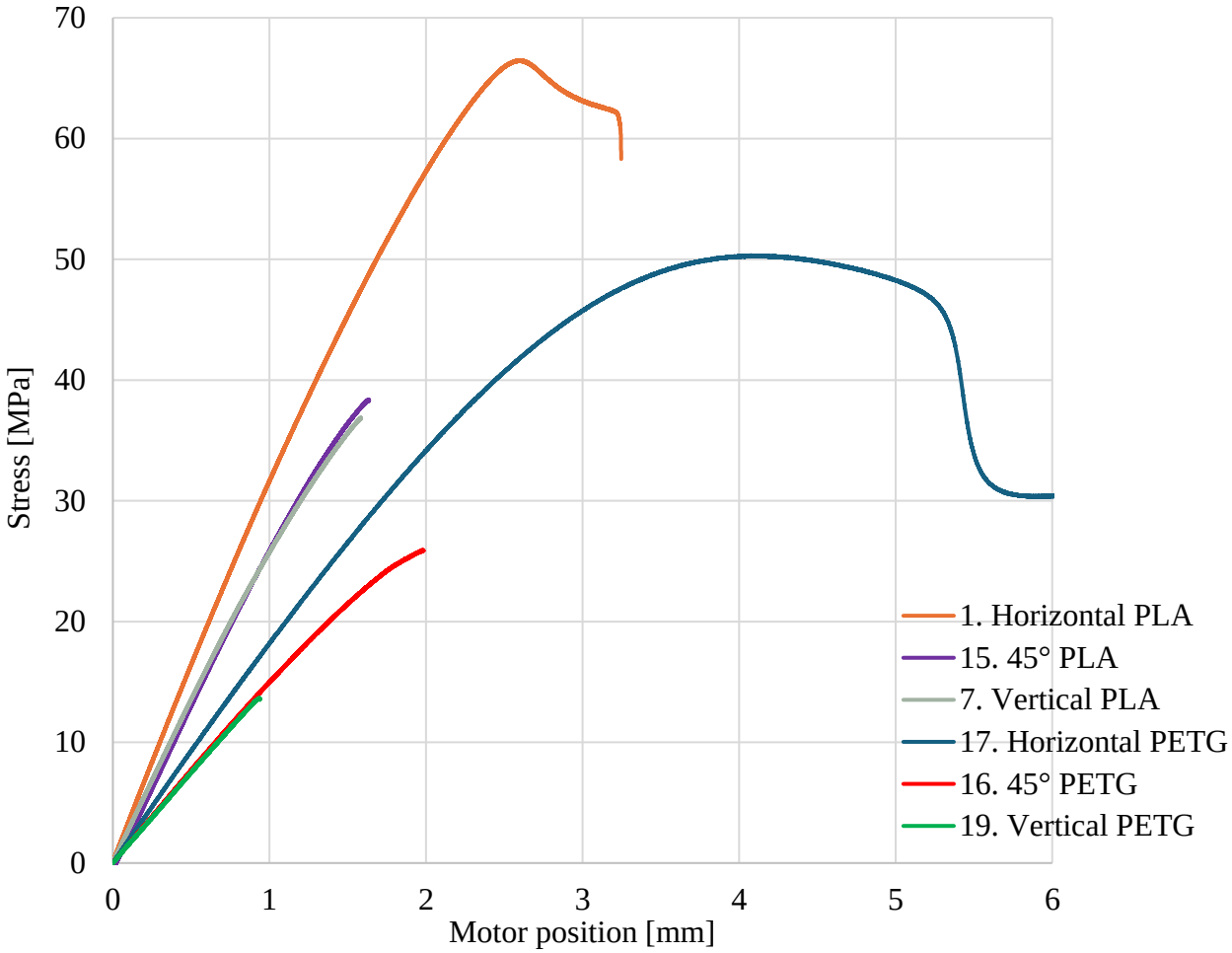

Figure 4.13. Stress–strain plot – Build orientation - Prusa

In next part comparison of AzteQ build orientation is given (Figure 4.14.). 45° one is lacking here but same trend can be seen. PLA horizontal orientation achieves 30 % higher ultimate load and stress values then comparative vertical series. PETG score 2.5 times higher.

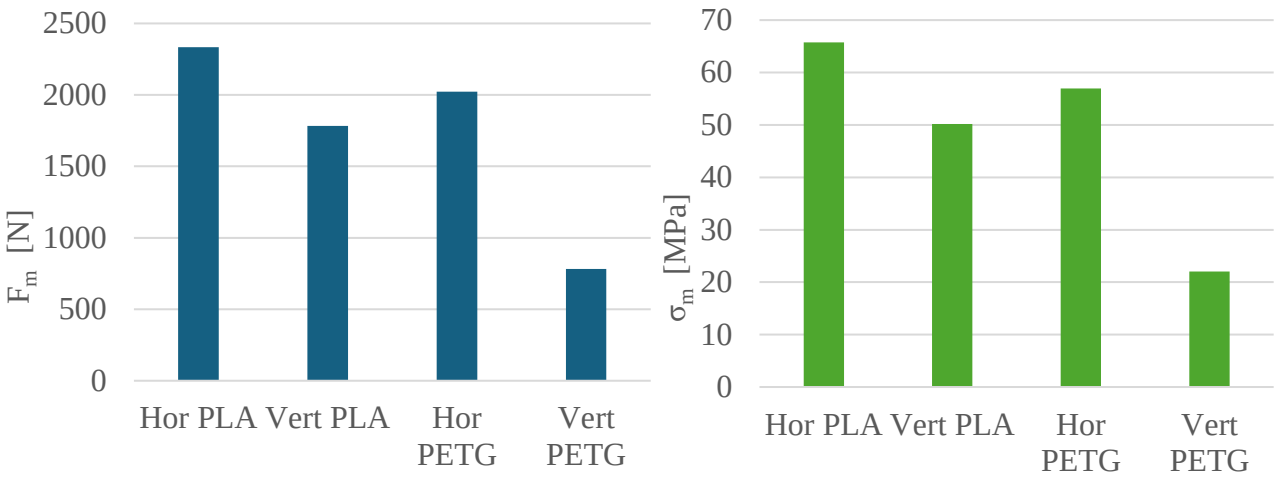

Figure 4.14. AzteQ - Ultimate strength load chart left, ultimate strength right charts

Figure 4.15. shows their corresponding Young's modulus of elasticity. Materials being tested having different properties shows different Young's modulus trends when variating orientation. In PLA horizontal has higher but for PETG, opposite pattern is noted.

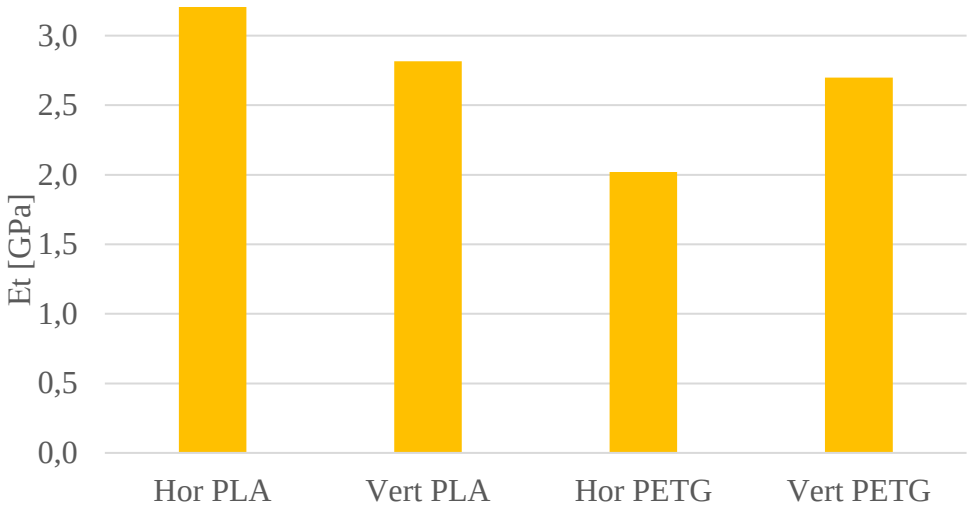

Figure 4.15. AzteQ - Modulus of elasticity chart

The stress-strain diagram in Figure 4.16. shows that fracture of vertically oriented specimens occurs at lower stress and strain values and exhibits characteristics of brittle material, breaking suddenly without a distinct yield point. In contrast, the curve for horizontally oriented samples resembles that

of conventional materials, displaying strain hardening after the yield point, followed by a necking region. To facilitate comparison on a single graph, the strain data for PLA was also represented in terms of motor position in this figure.

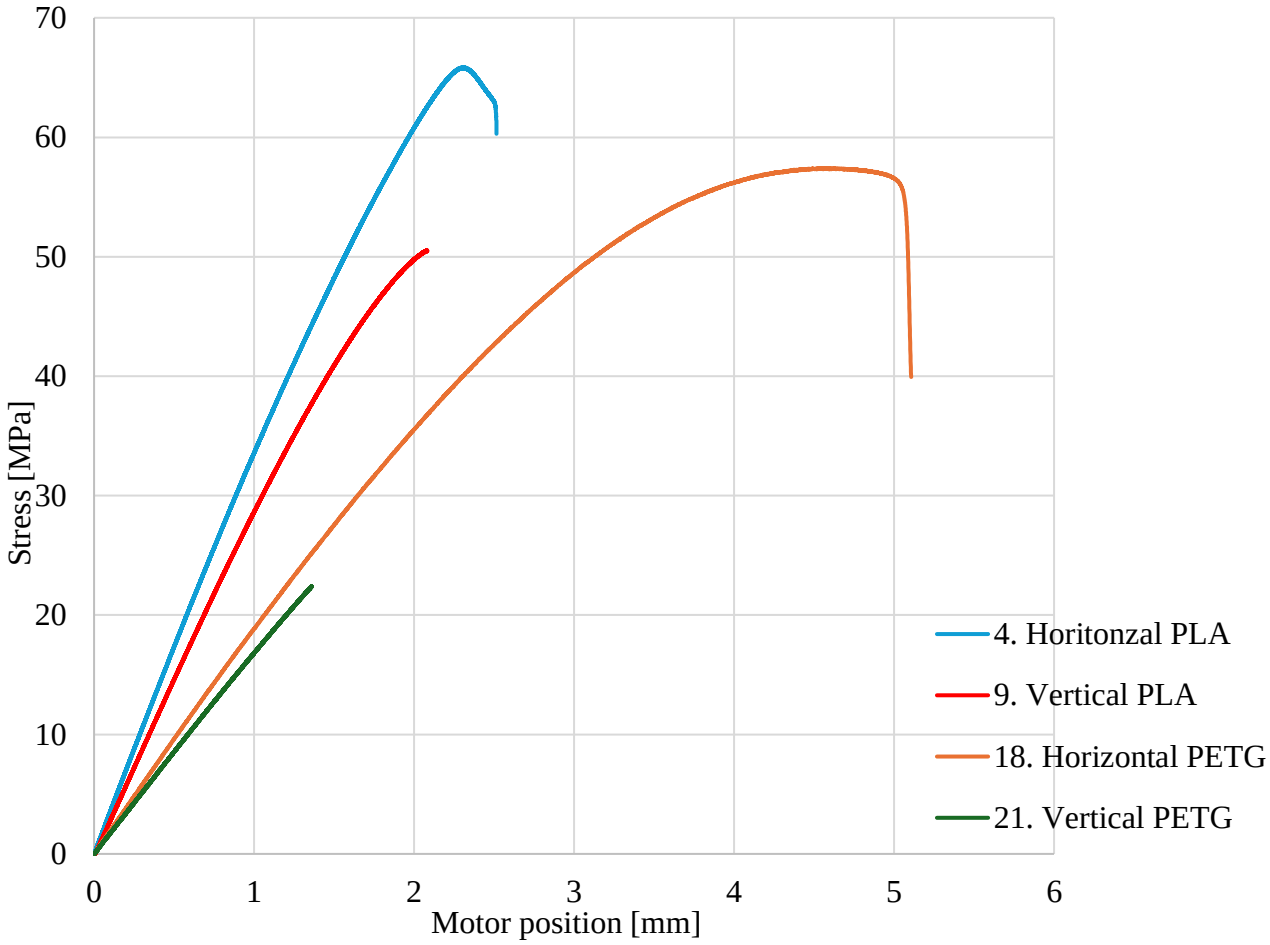

Figure 4.16. Stress–strain plot – Build orientation - AzteQ

The necking region is most pronounced in the elastic PETG specimens, where, after reaching the yield and ultimate strength points, the material continues to elongate almost indefinitely. Figure 4.17. illustrates one of these specimens undergoing testing on a UTM, clearly showing both elastic and plastic deformation regions. Unlike PLA, which fractures instantly, PETG demonstrates significant elongation due to its elastic properties. At the moment the photograph was taken, the elongation had exceeded 5 cm. Upon releasing the grips holding the specimen, it contracted slightly but remained permanently deformed.

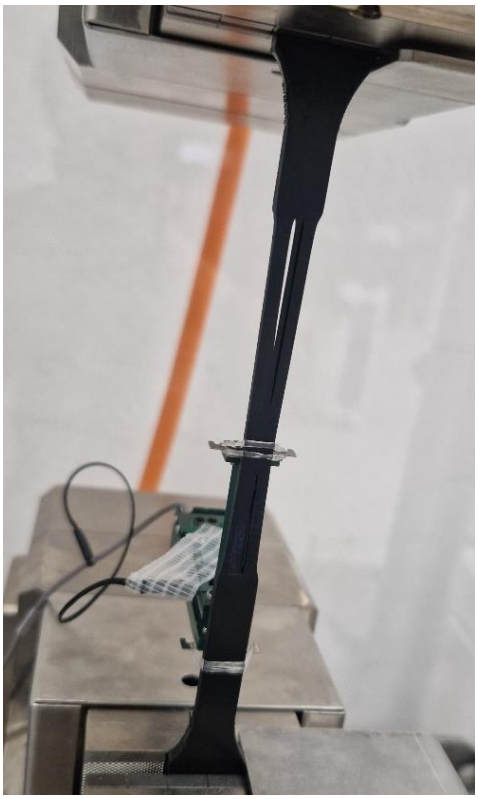

Figure 4.17. Series 17 - Horizontally printed PETG specimen

5. NUMERICAL MODEL

A numerical material model is a mathematical framework or set of equations used to describe the behaviour of materials under various conditions, such as stress, temperature, and time. Material models are essential in fields like engineering (eq. robotics), physics, and materials science to predict how materials will respond to external forces, deformations, or environmental changes. These models can range from simple linear elastic models, which assume that a material's deformation is proportional to the applied load, to more complex models like plasticity, viscoelasticity, or damage models, which account for non-linear behaviour, time-dependent effects, or material degradation [33].

Material models are used extensively in computational simulations, such as finite element analysis (FEA), to design structures, predict failures, and optimize materials for specific applications. Different types of material models are chosen based on the material's properties and the specific application or load conditions being studied [33].

5.1 Constitutive equations

Constitutive equations are mathematical relationships that describe how a material responds to external forces, deformations, or other physical influences, which is essential for solving complex engineering problems using FEM. These equations relate stress and strain (or other relevant quantities, such as temperature, electric field, etc.) in a material, defining its mechanical and physical behavior under various conditions. Constitutive equations are fundamental in material science and engineering because they provide the necessary link between material properties and the governing equations of mechanics (such as equilibrium equations) used in simulations and structural analyses [34].

Anisotropic, orthotropic, and isotropic are one of terms used to describe the mechanical and physical properties of a material, specifically how these properties vary with direction within the material. The property in question is material symmetry or directional dependence of properties such as elasticity, thermal conductivity, and strength. To calculate a numerical model for anisotropic, orthotropic and isotropic materials, different sets of material properties and data are required for each type due to their distinct characteristics [34]. Here's the data needed for each type:

Anisotropic Material have different properties in different directions, requiring elastic stiffness matrix (C_{ij}). A 6x6 matrix that defines stiffness in all directions with 21 independent constants (Young's modulus, shear modulus, Poisson's ratio in all directions) [34]. Generalized Hooke's Law for anisotropic material calculation is represented by:

$$\begin{Bmatrix} \sigma_x \\ \sigma_y \\ \sigma_z \\ \tau_{xy} \\ \tau_{yz} \\ \tau_{zx} \end{Bmatrix} = \begin{bmatrix} C_{11} & C_{12} & C_{13} & C_{14} & C_{15} & C_{16} \\ C_{12} & C_{22} & C_{23} & C_{24} & C_{25} & C_{26} \\ C_{13} & C_{23} & C_{33} & C_{34} & C_{35} & C_{36} \\ C_{14} & C_{24} & C_{34} & C_{44} & C_{45} & C_{46} \\ C_{15} & C_{25} & C_{35} & C_{45} & C_{55} & C_{56} \\ C_{16} & C_{26} & C_{36} & C_{46} & C_{56} & C_{66} \end{bmatrix} \begin{Bmatrix} \varepsilon_1 \\ \varepsilon_2 \\ \varepsilon_3 \\ \gamma_4 \\ \gamma_5 \\ \gamma_6 \end{Bmatrix} \quad (5.1)$$

Where:

σ_x, σ_y, σ_z are normal stresses,

τ_{xy}, τ_{yz}, τ_{zx} are shear stresses,

ε_x, ε_y, ε_z are normal strains,

γ_{xy}, γ_{yz}, γ_{zx} are shear strains,

C_{ij} are stiffness coefficients.

Orthotropic materials have three perpendicular planes of symmetry with different properties:

- Three Young's Moduli (E_x, E_y, E_z): Representing elasticity along three orthogonal axes;
- Three Shear Moduli (G_{xy}, G_{yz}, G_{zx}): Shear modulus in three orthogonal planes;
- Six Poisson's Ratios (ν_{xy}, ν_{yx}, ν_{yz}, ν_{zy}, ν_{zx}, ν_{xz}): For each pair of orthogonal directions [35].

Hooke's Law for orthotropic material looks like:

$$\begin{Bmatrix} \sigma_x \\ \sigma_y \\ \sigma_z \\ \tau_{xy} \\ \tau_{yz} \\ \tau_{zx} \end{Bmatrix} = \begin{bmatrix} C_{11} & C_{12} & C_{13} & 0 & 0 & 0 \\ C_{12} & C_{22} & C_{23} & 0 & 0 & 0 \\ C_{13} & C_{23} & C_{33} & 0 & 0 & 0 \\ 0 & 0 & 0 & C_{44} & 0 & 0 \\ 0 & 0 & 0 & 0 & C_{55} & 0 \\ 0 & 0 & 0 & 0 & 0 & C_{66} \end{bmatrix} \begin{Bmatrix} \varepsilon_1 \\ \varepsilon_2 \\ \varepsilon_3 \\ \gamma_4 \\ \gamma_5 \\ \gamma_6 \end{Bmatrix} \quad (5.2)$$

Isotropic materials have identical properties in all directions, only requiring:

- Young's Modulus (E): Modulus of elasticity representing stiffness.

- Poisson's Ratio (ν): Ratio of transverse to axial strain.
- Shear Modulus (G**):** Can be derived from Young's modulus and Poisson's ratio if not provided [35].

Hooke's Law for isotropic material consist of only two constants, C_{11} & C_{12}:

$$\begin{Bmatrix} \sigma_x \\ \sigma_y \\ \sigma_z \\ \tau_{xy} \\ \tau_{yz} \\ \tau_{zx} \end{Bmatrix} = \begin{bmatrix} \boldsymbol{C_{11}} & \boldsymbol{C_{12}} & \boldsymbol{C_{12}} & 0 & 0 & 0 \\ \boldsymbol{C_{12}} & C_{11} & \boldsymbol{C_{12}} & 0 & 0 & 0 \\ \boldsymbol{C_{12}} & \boldsymbol{C_{12}} & C_{11} & 0 & 0 & 0 \\ 0 & 0 & 0 & \dfrac{\boldsymbol{C_{11}} - \boldsymbol{C_{12}}}{2} & 0 & 0 \\ 0 & 0 & 0 & 0 & \dfrac{\boldsymbol{C_{11}} - \boldsymbol{C_{12}}}{2} & 0 \\ 0 & 0 & 0 & 0 & 0 & \dfrac{\boldsymbol{C_{11}} - \boldsymbol{C_{12}}}{2} \end{bmatrix} \begin{Bmatrix} \varepsilon_1 \\ \varepsilon_2 \\ \varepsilon_3 \\ \gamma_4 \\ \gamma_5 \\ \gamma_6 \end{Bmatrix} \tag{5.3}$$

Where C_{11} and C_{12} are fully defined by stress, strain, modulus of elasticity and Poisons coefficient [35].

5.2 Finite element analysis

Material model for a tensile test of FDM 3D-printed materials typically involves using a linear elastic model or a bilinear elastic-plastic model to represent the material's stress-strain behaviour. This approach captures the key mechanical properties of FDM-printed materials under uniaxial tension, focusing on elastic modulus, yield strength, and ultimate tensile strength. For a basic analysis, the linear elastic model assumes that the material behaves elastically up to failure. The stress-strain relationship is described by Hooke's Law given by formula (3.3). This model is suitable for materials and scenarios where the deformation remains within the elastic region, meaning that the material returns to its original shape after the load is removed. However, FDM-printed parts often exhibit complex behaviour due to their layer-by-layer construction, which can introduce anisotropy and different failure mechanisms [36].

A FEA of FDM 3D-printed materials involves simulating the mechanical behaviour of a part under various loading conditions by taking into account the unique characteristics of the FDM process,

such as layers bound together without material fusion (layer structure in the Figure 3.11. & 3.12.), anisotropy, and material heterogeneity. The goal of FEA in this context is to predict the performance, strength, and failure modes of the printed part, considering the complex internal structure introduced by the FDM process [37].

From the measurements obtained, we gathered data sufficient to fully characterize the material as isotropic. To describe the material as orthotropic, multiple extensometers are required to capture strain data in all three principal directions, along with the determination of three shear moduli through shear testing. Material properties needed to make FEA of isotropic material include elastic modulus, yield strength, ultimate tensile strength and fracture toughness. They all vary between the filament direction and the layer bonding direction [36].

FEA of the tested specimens was performed using Ansys software. The geometry was discretized into small mesh elements to approximate the behaviour of the part under load. For FDM, the mesh needs to be fine enough to capture details like the individual filament strands and layer boundaries, especially if layer anisotropy and bonding strength are considered [38]. Care was taken to avoid an overly fine mesh, which would significantly increase computation time, while still ensuring accuracy in the analysis.

Chosen series to take data for analysis are series 1. They are individually horizontally printed samples on Prusa with PLA material. The material was defined in the *Engineering Data* section of *Ansys Workbench* as Polyethylene, with updated values based on experimentally measured material properties. The corresponding data are presented in Table 5.1.

Table 5.1. Values used for FEA

ε_m [%]	σ_m [MPa]	σ_y [MPa]	E_t [GPa]
1	64,867	62,58	3,352

A strain of 1% was selected for the analysis, as this value falls within the linear region of the stress-strain curve, where the relationship adheres most consistently to Hooke's Law across all analyzed specimens. The remaining material properties were derived from Table 4.1, corresponding to the appropriate experimental series.

5.2.1 Developing a model

The objective of this section is to define the material properties of anisotropic 3D printed part as consisting of two isotropic materials. One material being the extruded lines with its values that are measured at the horizontal specimen (Table 5.1.). The second material is a bonding element between the layers, simulating the INFB.

Figure 5.1. shows the meshed model used for the analysis, which is simplified to two bonded single lines. The dimensions are consistent with those of two layers stacked one on top of the other, with a total height of 0.4 mm and a width of 0.2 mm. The adhesive middle layer, represented in orange in Fig. 40., is assumed as 10 % of total size. That makes it 0.02 mm thick, while the top and bottom perimeters are 0.19 mm each. The mesh size was set to 0.01 mm to accommodate the scaled-down model. Mesh used is 3D square elements, defined in Ansys as type “SOLID 186”.

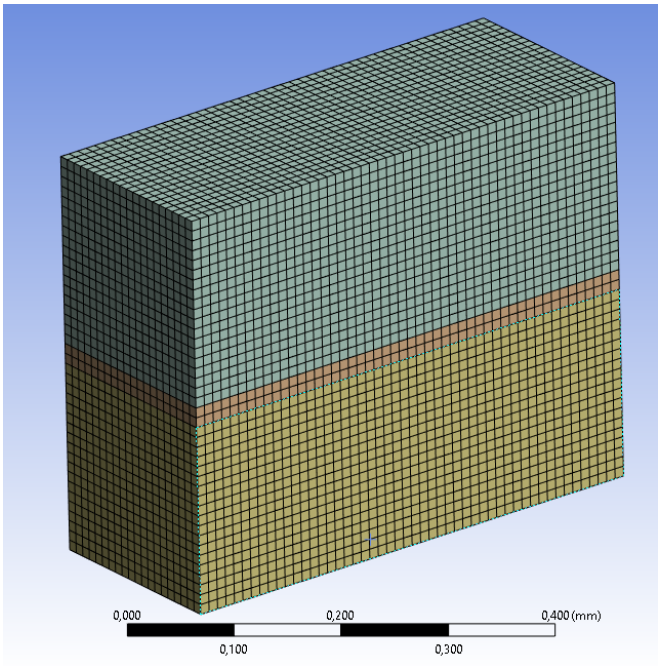

Figure 5.1. Vertical model

In the tensile testing measurements, force is applied, and strain is measured using an extensometer. However, in this simulation, the procedure is reversed: strain is applied through the *'remote displacement'* function in Ansys, and the resulting force reaction is calculated.

Since the model is scaled, the remote displacement must be calculated using equation (3.2):

$$\Delta L_0' = L' \cdot \varepsilon = 0{,}4\,mm \cdot 0{,}01$$

$$\Delta L_0' = 0{,}004\,mm$$

Where;

L_0' is the initial length of the model used in the FEM analysis,

$\Delta L_0'$ is the increase in the model length due to applied strain.

It's cross-section area is:

$$A' = 0{,}5 \cdot 0{,}2 = 0{,}1\,mm^2$$

For the scaled model to accurately represent the stress experienced by the actual component, the stress in the model (σ') must be equal to the stress in the part it represents (σ). Therefore, the following equation holds:

$$\sigma = \sigma' \tag{5.5}$$

Using stress formula (3.1) expected scaled force is calculated then:

$$\frac{F}{A} = \frac{F'}{A'}$$

$$F' = \frac{F}{A} A' = \frac{908}{35{,}51} \cdot 0{,}1$$

$$F' = 2{,}557\,N$$

This completes the definition of static structural analysis in Ansys and simulation can be executed. The modulus of elasticity for the extruded perimeters was set to 3.352 GPa, as calculated in the horizontal case, while the modulus of elasticity for the adhesive layer was varied. Optimizing through an iterative procedure, the material properties of the adhesive were systematically adjusted to develop a representative material model for the IFBS. This method ensured that the developed model accurately reflects the mechanical behavior of the material under the specified conditions.

It was determined that for E = 2.1 GPa of glue material, the model yielded a resulting force of 2.618 N. This value is 2% higher than the expected value obtained from tensile testing.

Figure 5.2. shows the equivalent stresses in the developed FEM model. As expected, the highest stresses were observed in the middle, concentrated in the adhesive layer, which has the lowest modulus of elasticity. The maximum recorded stress was 32.382 MPa.

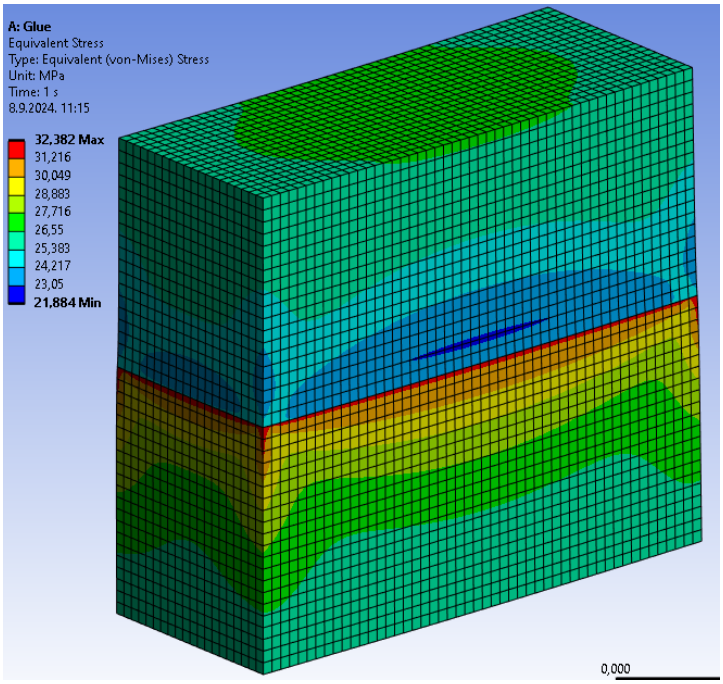

Figure 5.2. Von Mises Stress

5.2.2 Verification of the material model

Theoretically, if the material model from first study is valid, a model comprising multiple layers with varying build orientations should yield results consistent with the empirical values measured during the corresponding tensile tests.

To test this premise, a section of a 45° test sample was modeled, as shown in Figure 5.3. The model has dimensions of 1 mm in length, 0.4 mm in width, and 0.5 mm in height, consisting of six layers with bonds between them. The mesh size and type as well as material properties for both the layers and the adhesive were the same as those developed in the first study. This model is comparable to the printed test specimen from Series 15; printed on Prusa with PLA material with 45° specimen rotation.

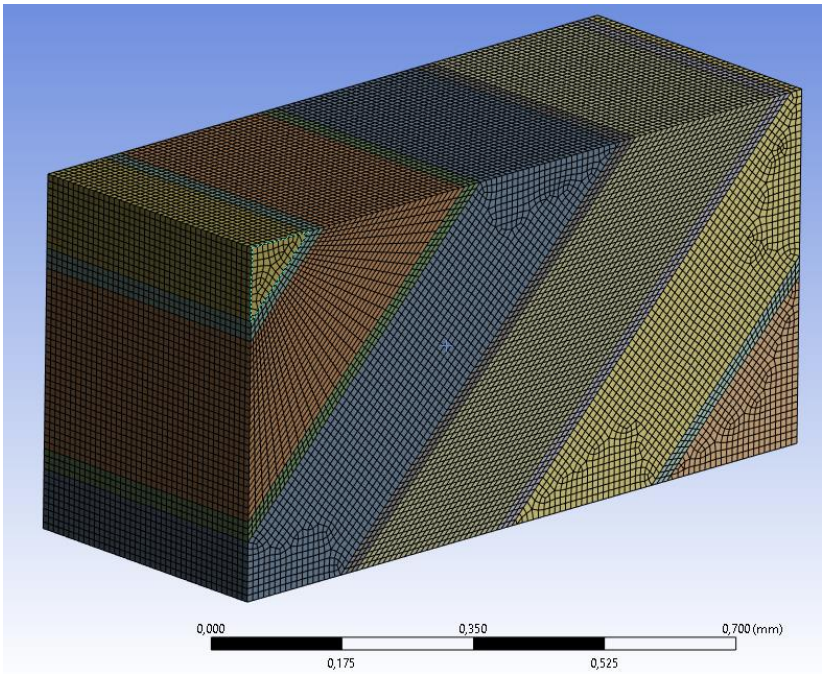

Figure 5.3. 45° meshed model

As model is different size then first study, therefore remote displacement needs to be determined again using formula (3.2):

$$\Delta L_0'' = L'' \cdot \varepsilon \; = \; 0{,}5\, mm \cdot 0{,}01$$

$$\Delta L_0'' = 0{,}005\ mm$$

It's cross-sectional area is:

$$A'' = 0{,}4 \cdot 0{,}1 = 0{,}4\ mm^2$$

Using the stress formula (5.6), the expected scaled force can be calculated as:

$$F'' = \frac{F}{A} A'' = \frac{1126{,}34}{35{,}51} \cdot 0{,}4$$

$$F'' = 12{,}688\ N$$

Figure 5.4. shows the von Mises stress distribution in the 45° FEM model. As expected, the stress values vary in a range between vertical and horizontal values at 1% strain, as the model is composed of elements with both orientations. Due to the multiple layers and their rotation relative to the applied remote displacement, some inevitable stress concentrations occur at the interfaces where different materials meet. This results in a maximum von Mises stress of 43 MPa. The average stress, however, is 31.564 MPa, which aligns with the behavior of horizontal specimen.

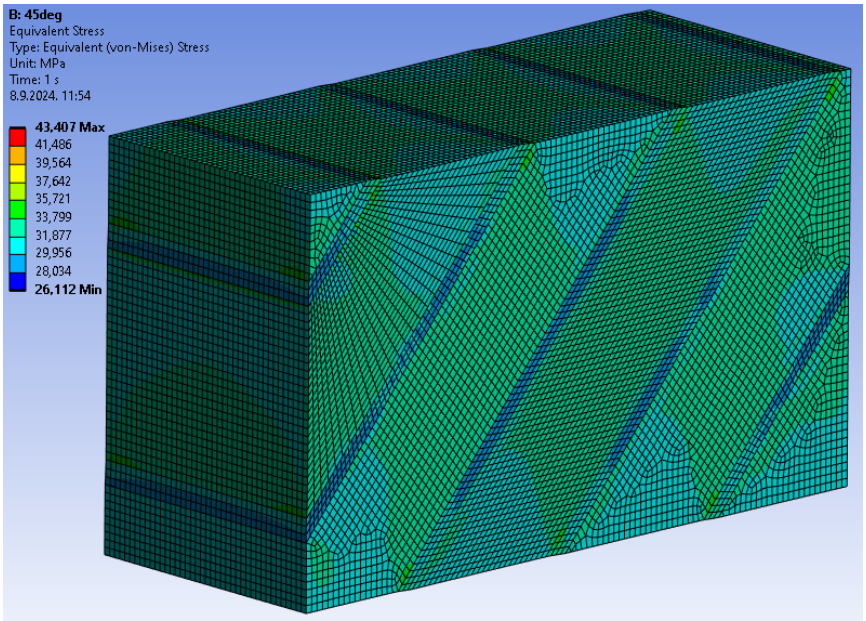

Figure 5.4. 45° Equivalent (von Mises) Stress

The force reaction reads 12.663 N, which is nearly identical to the expected scaled force of 12.688 N. The results from this study confirm that the proposed numerical model is suitable for predicting the material properties of FDM parts. This aligns with the primary goal of this paper: to develop a reliable predictive model that can accurately predict the behavior of 3D-printed parts when integrated into robotic assemblies. Same approach could be applied to PETG specimens.

Table 5.3. presents the values calculated by both simulations in comparison with those obtained from experimental testing. For the numerical model to be validated, these values must closely match. Both cases demonstrated good agreement with the experimental data. Simulated force for vertical case was 2.3 % higher than the measured value, while forces of 45° case matches almost perfectly.

Table 5.2. Comparison of measured values with FEM calculations

	Vertical		45°		
	Measured	FEM	Measured	FEM	Unit
$F_{1\%}$	908,26	929,65	1126,34	1124,16	N
$\sigma_{ekv1\%}$	32,382	25,567	31,720	43,407	MPa

It is important to emphasize that this FEA is valid only for the specific material, printer and print parameters used in this study. Any changes in material or equipment will require the development of a new model.

6. GUIDELINES

In last part of paper, few guidelines for successful AM FDM-s are given. They are synthesis from official guidelines given by standards [39] and research papers [30], extended with ones given by our own experience after this experiment.

6.1 Use of commercial materials in additive manufacturing

The document "ISO/ASTM 52910:2018" provides guidelines for designing parts to be produced by AM. It covers the unique design opportunities AM offers, such as creating complex and custom geometries without hard tooling, and the ability to optimize parts for specific functions using techniques like topology optimization. The standard also discusses limitations, such as the need for post-processing and challenges related to material properties and process variability, which can affect the quality and performance of AM parts [39].

The document provides several guidelines for designing parts for AM:

1. Design: Utilize the design freedom of AM, such as creating complex geometries and custom parts without the need for molds or fixtures.
2. Material Properties: Account for the anisotropy and variability in material properties specific to AM processes. Choose materials specifically developed or certified for AM processes. Study the mechanical, thermal, and chemical properties of commercial materials. Pay attention to how these properties change under the unique conditions of AM, such as thermal gradients or layer-by-layer deposition. Use materials from reputable suppliers with consistent quality and certifications. This reduces variability and ensures reliable performance. Verify that the selected material is compatible with your specific AM machine and process parameters. Adjust machine settings if necessary to accommodate the material's properties.
3. Post-Processing: Design parts to minimize or accommodate the need for post-processing, such as removing support structures.
4. Build Orientation: Consider the impact of build orientation on surface finish, strength, and dimensional accuracy.

5. Plan for Build Volume Constraints: Design within the machine's build envelope or consider part segmentation and assembly.

These guidelines help ensure parts are designed effectively to leverage the benefits of AM while addressing its limitations [39].

It is important to note that the default printing speeds for perimeters, infill, support structures, and other print features differ, which negatively impacts the uniformity of the printed part and complicates the prediction of its material properties. To improve consistency and simplify the prediction of material behavior, it is recommended to equalize the print speed across all features. Slower print time also increases its quality. Additionally, printing the entire part using only perimeters, rather than incorporating infill, can further enhance the predictability of the part's mechanical properties.

6.2 Applying research results to robotic components

Research results are categorized and explained here in five main categories relevant to robotic components:

Materials

PETG is generally more suitable for robotics applications than PLA. PETG's higher strength, durability, and flexibility make it ideal for parts that need to withstand mechanical stress, impacts, and potential exposure to various environmental conditions. It also has better temperature and chemical resistance and it's more resistant to outdoor conditions, which is beneficial in robotics, where components may be exposed to heat from motors or environmental factors. While PLA could be used for non-load-bearing or aesthetic parts in robotics, PETG is the better choice for functional components that require robustness and reliability. As PLA is easier to print and cheaper it's more suitable for prototype build then late do it from PETG [10] [11].

Printer

For prototyping purposes, both printers are sufficiently capable of producing parts for robotic applications. However, the AzteQ demonstrated superior performance, consistently producing parts with higher material properties across all tests. Therefore, for critical components that require maximum strength and precision, it is advisable to use a printer equipped with advanced features and constructed from high-quality components, such as the Trilab AzteQ Industrial.

Layer time

Considering the parameter of layer time, printing parts one at a time is recommended to achieve the highest possible quality for robotic components. This approach minimizes variations in layer cooling and bonding, leading to improved material strength and overall part performance.

Build orientation

Parts are stronger along the X and Y axes and weaker along the Z-axis due to the nature of layer bonding. For robotics parts that endure stress, orienting them to maximize strength in the direction of the applied forces is crucial. The orientation affects the quality of surfaces too, with top and bottom surfaces generally having better quality. Parts requiring precise fits or smooth surfaces should be oriented to reduce the need for supports, enhancing surface finish and reducing post-processing. Proper orientation can minimize the need for supports, reducing both print time and material usage. Efficient orientation is key for quick prototyping and material conservation in robotics applications.

FEA

Before printing critical robotic parts, developing a numerical model in advance is highly recommended. This approach allows for accurate predictions of material properties and mechanical behaviour before physical assembly, reducing the need for multiple design iterations and ensuring a more efficient production process. Numerical models help simulate the stresses, strains, and other mechanical characteristics of 3D-printed parts, particularly in FDM, where anisotropy and IFBS can significantly affect performance. By using such models, engineers can optimize print parameters, material selection, and design geometries, leading to more reliable and functional robotic components.

This process not only allows for material prediction that improves the accuracy and durability of the final parts, but also shortens the development cycle, resulting in cost-effective and timely production.

7. CONCLUSION

This study explored the impact of various Fused Deposition Modeling (FDM) parameters, such as printer setup, material choice, build orientation, and layer time, on the mechanical properties of 3D-printed components. The research confirmed that factors like tensile strength and interfacial bonding strength (IFBS) vary significantly depending on the printing conditions, demonstrating the complexity of predicting FDM part behaviour. Through tensile testing and analysis of PLA and PETG materials, the results provided practical insights into how key printing parameters affect performance, particularly in robotic applications where precision, strength, and prediction of material behaviour are critical.

Based on the data obtained from tensile testing following ISO 527 standards, a numerical model was developed. This model incorporates both extruded filament lines and bonding elements between layers, accurately representing the mechanical behaviour of 3D-printed parts with simple geometries. The findings contribute to a better understanding of how to optimize print parameters and predict material behaviour before robotic components are fully assembled. The constructed model was subsequently verified using an angled specimen to ensure its accuracy.

The study also highlights that increased layer time, caused by printing multiple parts simultaneously, leads to weaker interlayer bonds due to prolonged cooling intervals between subsequent layers. This finding confirms the hypothesis that longer layer times negatively affect bonding strength, suggesting that printing parts individually yields higher quality and more reliable components.

In conclusion, the study provides practical guidelines that can be applied to future designs, streamlining the process and ensuring the production of stronger, more reliable 3D-printed robotic parts.

REFERENCES

[1] Keleş Ö. et al, "Effect of build orientation on the mechanical reliability of 3D printed ABS," *Rapid Prototyping Journal,* vol. 23, no. 2, pp. 320-328, 2017.

[2] Yang L. et al., "Interlayer bonding strength of 3D printed PEEK," *Royal Society of Chemistry,* no. 17, pp. 4775-4789, 2021.

[3] Allum J. et al., "Interlayer bonding has bulk-material strength in extrusion additive manufacturing: New understanding of anisotropy," *Additive Manufacturing,* 2020.

[4] Khan S. et al., "A comprehensive review on effect of printing parameters on mechanical properties of FDM printed parts," *Materials Today,* 2021.

[5] Anderson. S. W. et al., "On the Effects of Process Parameters and Optimization of Interlaminate Bond Strength in 3D Printed ABS/CF-PLA Composite," *Polymers,* vol. 9, no. 12, pp. 2155-2171, 2020.

[6] Rodrı´guez F., "Design of Fused-Deposition ABS Components for Stiffness and Strength," *Journal of Mechnaical Design,* pp. 545-551, 2003.

[7] Fuller C. et al., "Interfacial Bonding Mechanism and Mechanical Performance of Continuous Fiber Reinforced Composites in Additive Manufacturing," *Chinese Journal of Mechanical,* no. 21, 2021.

[8] Bellini A. et al., "Mechanical characterization of parts fabricated using fused deposition modeling," *Rapid Prototyping Journal,* vol. 9, no. 4, pp. 252-264, 2003.

[9] ISO 527-1, *from internet, https://www.iso.org/standard/75824.html,* 20.8.2024..

[10] Prusament PLA filament, *from Internet, https://prusament.com/materials/pla/,* 20.08.2024..

[11] PRUSAMENT PETG filament, *from internet, https://prusament.com/materials/prusament-petg/,* 20.08.2024..

[12] Prusa i3 mk3s, *from Internet, https://www.prusa3d.com/product/original-prusa-i3-mk3s-3d-printer-3/#specs,* 20.08.2024..

[13] TRILAB AzteQ Industrial data sheet, *from Internet, https://trilab3d.com/3d-printer-azteq/,* 20.08.2024..

[14] Prusa mk3s specifications, *from Internet, https://printingit3d.com/is-the-prusa-i3-mk3s-worth-it-complete-printer-review/,* 20.08.2024..

[15] Trilab AzteQ review, *from Internet, https://www.techradar.com/pro/trilab-azteq-industrial-review,* 20.08.2024..

[16] ISO 527-2, *from Internet, https://www.iso.org/standard/56046.html,* 20.08.2024..

[17] Davis J. R., Tensile testing (2nd ed.), ASM International, 2004.

[18] Step LAB universal testing machine, *from Internet, https://step-lab.com/systems-based-on-electromechanical-actuators/,* 20.08.2024..

[19] Extensometers Zwick/Roell, *from Internet, https://www.zwickroell.com/accessories/extensometers/,* 20.08.2024..

[20] Extensometer Epsilon 3442, *from Internet, https://www.epsilontech.com/products/axial-extensometers/low-profile_extensometer-model-3442-overview/,* 20.08.2024..

[21] ASTM D638, *from internet, https://www.astm.org/d0638-14.html,* 20.08.2024..

[22] Mechanical Properties of Materials, *from internet, https://mechanicalc.com/reference/mechanical-properties-of-materials#stress-strain-approx,* 20.08.2024..

[23] Kellog T. et al., "Prediction of stress–strain diagram from forming load in stretch forming," *Mechanical Sciences,* pp. 46-53, 2012.

[24] Hot End Heat Creep, *from internet, https://www.xometry.com/resources/3d-printing/heat-creep/,* 20.08.2024..

[25] Boschetto L. A. et al., "Accuracy prediction in fused deposition modeling," *The International Journal of Advanced Manufacturing Technology,* vol. 73, p. 913–928, 2014.

[26] Akca E. T., "Metallographic Procedures and Analysis – A review," P*eriodicals of Engineering and Natural Sciences,* vol. 3, no. 11, 2015.

[27] Dino-Lite AM7013MZT, *from Internet, https://www.dino-lite.com/products_detail.php?index_m1_id=9&index_m2_id=36&index_id=48,* 20.08.2024..

[28] Understanding the extruded profile, *from Internet, https://dyzedesign.com/2018/07/3d-print-speed-calculation-find-optimal-speed/,* 20.08.2024..

[29] Smith A. et al., "Anisotropic material properties of fused deposition modeling ABS," *Rapid Prototyping Journal,* vol. 8, no. 4, pp. 248-257, 2002.

[30] Muller O. A. et al., "Optimization of fused deposition modeling process parameters for dimensional accuracy using I-optimality criterion," *Measurment,* vol. 81, pp. 174-196, 2016.

[31] Tymrak M. et al., "Mechanical properties of components fabricated with open-source 3-D printers under realistic environmental conditions," *Materials & Design,* no. 58, pp. 242-246, 2014.

[32] Rayegani G. et al., "Fused deposition modelling (FDM) process parameter prediction and optimization using group method for data handling (GMDH) and differential evolution (DE)," *The International Journal of Advanced Manufacturing Technology,* vol. 73, pp. 509-519, 2014.

[33] da Silva L. et al., Handbook of Adhesion Technology, Springer, 2011.

[34] Lekhnitskii S. G., Theory of Elasticity of an Anisotropic Elastic Body, Holden-Day, 1963.

[35] Gibson R. F., Principles of Composite Material Mechanics, CRC Press, 2016.

[36] Bhandari S. et al., Finite element analysis of thermoplastic polymer extrusion 3D printed material for mechanical property prediction, New Orleans: Elsevier, 2017.

[37] Gordson F. et al., "Computation of Mechanical Properties of Parts Manufactured by Fused Deposition Modeling Using Finite Element Method," *Springer International,* pp. 403-414, 2015.

[38] Moaveni S., Finite Element Analysis: Theory and Application with ANSYS, Pearson, 2014.

[39] ISO/ASTM 52910:2018, from Internet, https://www.iso.org/standard/67289.html, ISO, 2018.

[40] Rodríguez F., "Mechanical behavior of acrylonitrile butadiene styrene (ABS) fused deposition materials. Experimental investigation," *Rapid Prototyping Journal,* vol. 7, no. 3, pp. 148-158, 2001.

[41] Ishak B. et al., "Multiplane fused deposition modeling: a study of tensile strength," *Mechanics Based Design of Structures and Machines,* vol. 47, no. 5, pp. 583-598, 2019.

[42] Sood K. et al., "Parametric appraisal of mechanical property of fused deposition modelling processed parts," *Materials & Design,* vol. 31, no. 1, pp. 287-295, 2010.

[43] Schneider J., Concurrent geometrico-topological tuning of nanoengineered auxetic lattices fabricated by material extrusion for enhancing multifunctionality: Multiscale experiments, finite element modeling and data-driven prediction, Glassgow: Additive Manufacturing, 2024.

[44] Lee C. S.; Kim S.G.; Kim H.J., "Measurement of anisotropic compressive strength of rapid prototyping parts," *J Mater Process Technol,* Vols. 187-188, pp. 627-630, 2007.

[45] Lan T. et al., "Prediction of interfacial tensile bond strength in 3D printed concrete based on a closed-form fracture model" *Journal of Building Engineering,* vol. 70, 2023.

LIST OF LABELS AND ABBREVIATIONS

AM	Additive Manufacturing
AI	Artificial Intelligence
ABS	Acrylonitrile Butadiene Styrene
CF	Carbon Fiber
FDM	Fused Deposition Modelling
FEA	Finite Element Analysis
FEM	Finite Element Method
IFBS	Interfacial Bonding Strength
MEAM	Material Extrusion Additive Manufacturing
PETG	Polyethylene Terephthalate Glycol
PLA	Polylactic Acid
RP	Rapid Prototyping
UTM	Universal Testing Machine

ABSTRACT

Preliminary observations suggest that 3D-printed robotic parts exhibit varying performance based on printing conditions, prompting a methodological investigation into commercial materials for additive manufacturing. The objective of this study is to explore the effects of main factors in Fused Deposition Modeling (FDM) and to test the hypothesis that 3D-printed parts can be accurately represented using numerical models developed from simple geometries.

Tensile tests were conducted on PLA and PETG specimens, produced using different printer setups and part orientations, following the ISO 527 standard. The study examines how these variables influence material properties such as tensile strength and interfacial bonding strength (IFBS). The findings highlight significant variations in mechanical properties across different setups, providing practical design criteria for achieving specific reliability levels in additively manufactured components.

This research is unique in presenting reliable, measurable data on the performance of commercially available 3D printers, enhancing the understanding and optimization of FDM-printed parts. The results contribute to the development of a numerical model that can reliably predict the behavior of precise robotic components, thus streamlining the design process and improving part performance.

Keywords: 3D Printing, Additive manufacturing (AM), Fused Deposition Modelling (FDM), Finite Element Analysis (FEA), Finite Element Method (FEM), Interfacial Bonding Strength (IFBS), Material Extrusion Additive Manufacturing (MEAM)

SAŽETAK

Preliminarna opažanja sugeriraju da 3D-printani robotski dijelovi pokazuju različite performanse ovisno o uvjetima printa, što je potaknulo metodološko istraživanje komercijalnih materijala za aditivnu proizvodnju. Cilj ove studije je istražiti učinke ključnih faktora u *Fused Deposition Modelingu* (FDM) i testirati hipotezu da se 3D-printani dijelovi mogu točno prikazati pomoću numeričkih modela razvijenih na osnovnim geometrijama.

Vlačna ispitivanja provedena su na PLA i PETG uzorcima, proizvedenim korištenjem različitih postavki printera i orijentacija dijelova, u skladu sa standardom ISO 527. Studija ispituje kako ovi faktori utječu na svojstva materijala poput vlačne čvrstoće i međuslojne čvrstoće (IFBS). Rezultati ukazuju na značajne varijacije u mehaničkim svojstvima među različitim postavkama, pružajući praktične kriterije dizajna za postizanje specifičnih razina pouzdanosti u aditivno proizvedenim komponentama.

Ovo istraživanje jedinstveno je po pružanju pouzdanih, mjerljivih podataka o performansama komercijalno dostupnih 3D pisača, čime se poboljšava razumijevanje i optimizacija FDM-printanih dijelova. Rezultati doprinose razvoju numeričkog modela koji može pouzdano predvidjeti ponašanje preciznih robotskih komponenti, čime se pojednostavljuje proces dizajna i poboljšavaju performanse dijelova.

Ključne riječi: 3D ispis, aditivna proizvodnja (AM), Fused Deposition Modeling (FDM), analiza konačnih elemenata (FEA), metoda konačnih elemenata (FEM), međuslojna čvrstoća veza (IFBS), aditivna proizvodnja ekstrudiranjem materijala (MEAM).

LIST OF FIGURES

LIST OF TABLES